

AD-A952704

DTIC FILE COPY

Copy 3  
OCT 18 1963

# PROJECT SQUID

TECHNICAL REPORT MIT-28-T-P

AN EXPERIMENTAL INVESTIGATION OF A  
MAGNETOGASDYNAMIC ACCELERATOR

by

William T. Hogan

PRINCETON UNIVERSITY  
THE J. H. JOHNSON  
RESEARCH CENTER  
LIBRARY

MASSACHUSETTS INSTITUTE OF TECHNOLOGY

Cambridge, Massachusetts

DTIC  
ELECTRIC  
NOV 22 1963  
A

Project SQUID is a cooperative program of basic research relating to  
Jet Propulsion. It is sponsored by the Office of Naval Research and  
is administered by Princeton University through Contract Nonr1858(25),  
NR-098-038.

April 1962

This document has been approved  
for public release and sale its  
distribution is unlimited.

83 11 22 118

AD-276060

Technical Report MIT-28-T-P

PROJECT SQUID

A COOPERATIVE PROGRAM  
OF FUNDAMENTAL RESEARCH  
AS RELATED TO JET PROPULSION  
OFFICE OF NAVAL RESEARCH, DEPARTMENT OF THE NAVY

Contract Nonr1858(25), NR-098-038

AN EXPERIMENTAL INVESTIGATION OF A MAGNETOGASDYNAMIC ACCELERATOR

by

William T. Hogan

Massachusetts Institute of Technology

Cambridge, Massachusetts

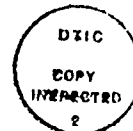
April 1962

PROJECT SQUID HEADQUARTERS  
JAMES FORRESTAL RESEARCH CENTER  
PRINCETON UNIVERSITY  
PRINCETON, NEW JERSEY

Reproduction, translation, publication, use and disposal in  
whole or in part by or for the United States Government is permitted.

This document has been approved  
for public release and its  
distribution is unlimited.

This paper was presented in part at the  
Third Annual Symposium on the Engineering Aspects of Magnetohydrodynamics  
in Rochester, New York, on 29 March 1962  
and should appear in the Proceedings of the meeting.



A-1

1

## AN EXPERIMENTAL INVESTIGATION OF A MAGNETOGASDYNAMIC ACCELERATOR

by

WILLIAM TIMOTHY HOGAN

Submitted to the Department of Mechanical Engineering on  
January 19, 1962 in partial fulfillment of the requirements  
for the degree of Doctor of Science.

### ABSTRACT

In the experiments to be reported, a d.c. crossed-field accelerator was attached to the downstream end of a 1.5" diameter combustion driven shock tube using either argon or air as the working fluid. The applied magnetic field was varied from 0 to 15 kilogauss, and the electrical power from 0.5 to 11 megawatts. By means of the  $\vec{J} \times \vec{B}$  body force, the shock heated gases were accelerated to a maximum of three times their original velocity. The increase in shock front and gas speed was measured from photographs of the flow taken with a rotating mirror camera, and ionization gages. The measured open circuit voltages were found to be a few percent lower than the ideal values for the circular channel. The electrical power supplied to the test gas was determined from simultaneous measurements of the voltage and current. The electrical conductivity of the plasma was measured upstream and downstream of the accelerator by the magnetic induction technique.

By apportioning the current between the test gas and the cooler gases that follow, the momentum and energy could be balanced. The momentum and energy conversion efficiency were found to be in the range of 60 percent to 90 percent and 40 percent to 70 percent, respectively. With the exception of a few percent, all of the electrical energy delivered to the test gas could be accounted for by summing the increase in kinetic energy of the test gas, the energy loss due to the electrode voltage drop, ohmic heating, and the energy associated with the high current densities in the Hartmann boundary layer.

The shock heated test gas upstream from the accelerator was about 15 percent ionized and had a velocity of about 4100 meters/sec., a Hall parameter  $\omega_e \tau_e < 1$ , an interaction parameter  $(\sigma B^2 / \rho u)$  of about 1 and a magnetic Reynolds number of about 0.5, the latter two parameters are based on the tube radius. The electrodes were made of copper strips and the current averaged over their surface had a maximum value of 500 amps/cm<sup>2</sup>.

Thesis Supervisor:

James A. Fay

Title:

Professor of Mechanical Engineering

## TABLE OF CONTENTS

ABSTRACT

TABLE OF CONTENTS

LIST OF SYMBOLS

I.	Introduction	1
II.	Experimental Equipment	15
III.	Data Presentation and Discussion	26
IV.	Conclusions	65
	Appendix A	68
	References	74
	Figures	76

# LIST OF SYMBOLS

a	area
A	cross sectional area of shock tube
B	magnetic field intensity
$B_0$	applied magnetic field intensity
E	electric field strength
e	charge on an electron
f	ratio of "heating power" to "pushing power"
G	mass flow rate
H	enthalpy
h	equivalent electrode separation distance
$I$	interaction parameter
J	applied current
$J_T$	total current
$J_s$	current flowing through test slug (Region 2)
$J_{2A}$	current flowing through Region 2A
j	current density
$j_\infty$	current density in the free stream
K	channel loading parameter
L	electrode axial length
$\mathcal{L}$	characteristic length
$l$	test slug length
$l_{b.l.}$	interaction length
M	mass of test slug
$\dot{m}$	mass flow rate

$m_o$  mass per atom  
 $n$  number density  
 $P$  pressure  
 $q_o$  ionization potential per atom  
 $R$  gas resistivity  
 $R_g$  resistance of gas in electrode gap  
 $R_m$  magnetic Reynolds number  
 $r$  tube radius  
 $T$  temperature  
 $t$  time  
 $t_m$  measured residence time of slug in gap  
 $t_J$  time duration of current flow  
 $u, u_g$  gas velocity  
 $\Delta u$  increase in gas velocity across accelerator  
 $V_s$  original upstream shock front velocity  
 $\Delta V_s$  increase in shock front velocity across accelerator  
 $\Delta V_{s_{ave}}$  average value of  $\Delta V_s$   
 $\Delta V_{s_p}$  peak value of  $\Delta V_s$   
 $\Delta \psi$  electrode surface voltage drop

#### Greek Symbols

$\delta_H$  Hartmann thickness  
 $\eta$  energy conversion efficiency  
 $\mu_o$  permeability of free space  
 $\mu$  viscosity of fluid  
 $\rho$  mass density, sometimes expressed as mm Hg at room temperature  
 $\sigma$  electrical conductivity  
 $\tau_e$  mean electron collision time

$\tau_{IN}$  ion-neutral collision time

$\phi$  potential drop across electrodes

$\omega_e$  electron cyclotron frequency

$\omega_I$  ion cyclotron frequency

Subscripts

1 initial conditions in driven section of shock tube

4 initial conditions in driver of shock tube

2 calculated conditions behind shock



## I. INTRODUCTION

Various electrical propulsion schemes have been proposed during the past several years as possibilities for substantially reducing the initial ground level launch weight requirements for propelling large payloads into space. Once a vehicle has achieved a low earth orbit by means of the conventional chemical rockets, a high thrust level is no longer necessary. If an electrical propulsion device could be used after the low orbit is reached, the weight of payload that could be propelled into higher orbits (near space missions) could be increased by at least a factor of two<sup>(1)</sup>.

It is to be noted that electrical propulsion differs markedly from chemical propulsion in the sense that in the former the source of power and the working fluid are separate items. As a result, the optimum specific impulse for an electrical propulsion system is not the highest obtainable value as in the case of a chemical rocket. The optimum performance is obtained when the total weight of the propellant and power plant is minimized. For electric propulsion schemes the propellant weight decreases with increasing specific impulse. Based on estimates of the specific weights of power plants that are likely to be available in the next few years, the optimum specific impulse for missions within the gravitational field of the earth is within the range 1000 to 5000 seconds. For interplanetary flights the optimum specific

impulse is within the range 7500 to 10,000 seconds<sup>(1)</sup>.

The various electrical propulsion systems that have been proposed may be classified as electrostatic accelerators (ion beam devices), or neutral plasma devices. In the ion beam devices, atomic ions are formed and accelerated to the desired velocity in an electric field. It appears<sup>(1)</sup> that a lower limit of about 7500 seconds must be placed on the specific impulse for ion beam devices due to practical considerations based upon the effects of electrode erosion by heavy ion bombardment, radiation from hot surfaces and ion space charge current limitation in the accelerating region.

In the neutral plasma devices, the ion and electron densities are essentially kept equal so that the space charge limitations of the ion beam devices is avoided. Energy can be transmitted to the plasma either by Joule heating, thus increasing the thermal energy of the gas, or by having a current flow in the plasma in the presence of a magnetic field, thus producing a body force which accelerates the plasma and increases the energy of directed motion of the gas.

The first of these energy transfer mechanisms is utilized in the arc jet. In this device, the propellant gas is heated as it flows through an electric arc. The hot gas is then expanded in a nozzle. The frozen flow losses; that is, loss of energy that has been invested in dissociation and ionization increases with specific impulse and for efficient operation of the arc jet an upper limit of about 1500 seconds must be imposed on the specific impulse.

The second of the above mentioned energy transfer mechanisms suggests the possibility of a number of propulsion schemes since there are a variety of ways in which magnetohydrodynamic forces can be made to act on a plasma. Since in these devices kinetic energy rather than thermal energy is added to the gas, frozen flow losses may be minimized. Of the variety of magnetohydrodynamic devices, the one considered in this paper is a viscously contained accelerator having an applied current and magnetic field mutually perpendicular to each other and to the flow (see Figure 1). Before entering the accelerator, the propellant gas would be preheated by an arc jet. The electric currents in the presence of the magnetic field produce a force ( $\vec{J} \times \vec{B}$ ) which accelerates the gas. This accelerating force is perpendicular to the magnetic field and to the electric current. This device appears to be able to extend the specific impulse range of the arc jet from 1500 seconds to about 5000 seconds. As was previously noted, this is the range for the optimum specific impulse for missions within the Earth's gravitational field.

For the type of accelerator under consideration, analytical studies by Fay, Janes, and Keck<sup>(2)</sup> have shown that there exists a minimum power level of the order of a few tenths of a megawatt below which the total losses inherent in this acceleration technique are comparable with

the ideal power and operation becomes marginal. The objectives of the experimental program were to achieve high levels of specific impulse and power and to measure the overall performance characteristics of the device. The power level was to be high in the sense that the total energy losses should represent only a small fraction of the input power, thus the device was to be operated at several megawatts.

For the experimental program a 1.5" combustion driven shock tube was used as a source of hot ionized gas, rather than the far more elaborate and expensive steady flow arc jet. With this equipment a limited amount of gas is heated and set into motion by a shock wave that is propagated down the tube. The shock tube characteristics impose an unfortunate limitation on the maximum testing time (less than 100  $\mu$ sec.) and minimum density for operating the accelerator. At initial tube densities ( $\rho_1$ ) lower than 1 mm Hg in argon or air the length of test gas behind the shock front becomes unreasonable short, being less than a tube diameter. As a result the available equipment did not provide the possibility of a steady flow experiment; only a slug flow could be produced. Thus no attempt was made to tailor the device to fit the demands of the various possible analytical steady flow gas dynamic solutions such as constant temperature and electric field, constant temperature and magnetic field, or constant electric and magnetic fields. Furthermore, the slug flow restricts the experimental measurements to overall performance

characteristics. A far more elaborate steady-state device would be needed to allow measurements to be made of the more fundamental variables through the length of the accelerator. Some experiments have been conducted with the magnetogasdynamic accelerator using steady flow<sup>(4,5,6)</sup> but these have, in general, been limited to rather low power levels. To date, these have also dealt only with the overall performance characteristics.

#### Operating Limitations and Losses

The design of the magnetohydrodynamic accelerator is influenced not only by the gas dynamics, but also by a group of auxiliary effects which collectively may control the range of possible operation. These include the gas conductivity, Hall currents, ion slip, electrode loss, boundary layer loss, electrode end losses, applied magnetic field loss, frozen flow losses, and leaving losses<sup>(2)</sup>. Since, in general, the experimental equipment must be tailored to meet requirements set by the first five effects, these will be examined in detail below. Concerning the other effects, it is noted that the electrode end loss depends on the shaping of the magnetic field at the entrance and exit and may be kept to a low value by extending the magnetic field somewhat beyond the electrodes<sup>(3)</sup>. The applied magnetic field loss (and also the electrode loss) can be made small by having a short length and large cross-section. The frozen flow and leaving loss are determined by the thermodynamics of the working fluid (propellant) and need not be of primary concern to this experimental program.

# (1) Joule Heating Loss and Electrode Length

The "Lorentz Force" integrated over the channel length (L) for a constant area channel gives the momentum flux leaving the channel, neglecting viscous losses, as:

$$(\vec{J} \times \vec{B})L = \dot{m}(u - u_{in}) \quad (1)$$

where  $\dot{m}$  is the mass flow rate,  $u$  is the exit velocity, and  $u_{in}$  is the entrance velocity. If it is assumed that the exit velocity is large compared to the entrance velocity, then the channel length is given by the expression:

$$L = \frac{\dot{m}}{\sigma_B^2} \frac{1}{f} \quad (2)$$

where  $f$  is defined by the expression  $f = \frac{j}{\sigma_{UB}}$ . Assuming no ion slip,  $f$  is just the ratio of heating power input ( $j^2/\sigma$ ) to acceleration power input ( $jBu$ ), and thus to demonstrate the operation of a magnetic accelerator  $f$  must be much less than unity.

For steady flow to be achieved in the shock tube accelerator, it would be necessary that the accelerator length (L) be made very small compared to the length of the test gas slug ( $l$ ). Table I shows the dependence of  $f$  on the initial density ( $\rho_1$ ), shock velocity ( $V_s$ ), and accelerator length for the interesting case of maximum Lorentz Force\* and

---

\*It is assumed here that the magnetic fields that can be applied in the laboratory are presently limited to about 15,000 gauss and the applied current is limited to about 25,000 amps.

minimum density (maximum velocity increase), that can be achieved using argon as the working fluid.

Thus with the available equipment it is not possible to produce substantial magnetohydrodynamic acceleration of the test gas ( $\Delta V_s$  equivalent to specific impulses of about 1000 sec.) by means of operating at the lowest densities and highest obtainable Lorentz Force and at the same time approach steady flow by making the accelerator length an order of magnitude shorter than the length of the test gas slug, for under these conditions  $f$  exceeds unity. If the

TABLE I

$\rho_1$ mm.Hg	$V_s$ m/sec.	$\frac{l}{d}$	$f$ $L = \frac{1}{10}l$ $L = l$		Ideal Power for $f \ll 1$ Steady Flow Megawatts	Ideal $\Delta V_s$ for $f \ll 1$ Steady Flow Equivalent Specific Impulse m/sec.   sec.	
1	5450	2.6	3.4	.34	22	11,540	1180
1	4800	2.5	4.5	.45	23	12,560	1280
1	3200	2.1	18.0	1.80	36	26,000	2660
2	4800	4.0	3.0	.30	16	7,560	775
3	4500	13.0	1.0	.10	13	5,420	555

POSSIBLE RANGE OF EXPERIMENTS IN 1.5" SHOCK TUBE USING  
ARGON AS WORKING FLUID  
( $d$  = tube diameter)

objective of substantial magnetic acceleration of the gas is to be achieved, then the accelerator length must be made at least as long as the slug in order to maintain  $f$  reasonably

less than unity. In the experiments to be reported herein, two accelerator lengths were used; one about twice the slug length, and the other four times the slug length.

## (2) Hall Currents

At high magnetic field strength, the electrons follow curved paths between collisions due the  $(\bar{v}_e \times \bar{B})$  force. Thus, the electrons tend to drift in a direction perpendicular to the net electric field and to the magnetic field. If, in Figure 1, the current is assumed to flow in the y-direction, then the current density and the electric field are related by:

$$E_y - u_1 B = j_y / \sigma \quad (3A)$$

$$E_x = (\omega_e \tau_e) \frac{j_y}{\sigma} \quad (3B)$$

where  $\omega_e \tau_e$  is the product of the electron cyclotron angular frequency and the mean electron collision time, and is given by the expression  $\omega_e \tau_e = \frac{\sigma B}{n_1 e}$ .

Thus, at sufficiently large values of  $\omega_e \tau_e$  the longitudinal field ( $E_x$ ) could be larger than the transverse field, in which case steps must be taken to prevent discharge of the Hall field ( $E_x$ ) through the boundary layer. If there is no "Hall" field established; that is, the Hall currents are allowed to flow, then the full expression for Ohm's law for the case of orthogonal magnetic and electric fields shows that two components of the current exist, namely,



$$j_y = \frac{\sigma(E - u_1 B)}{1 + (\omega_e \tau_e)^2} \quad (4A)$$

$$j_x = \frac{\sigma \omega_e \tau_e (E - u_1 B)}{1 + (\omega_e \tau_e)^2} \quad (4B)$$

The longitudinal component of the current, or Hall current, effectively reduces the axial component of the body force by the factor  $\frac{1}{1 + (\omega_e \tau_e)^2}$  and also introduces a transverse component of the body force.

One method that has been suggested to prevent Hall currents from flowing in a practical machine is to use segmented electrodes; that is, a series of electrodes in the axial direction electrically insulated from one another so that a Hall field is established<sup>(7)</sup>.

In general, the Hall effect becomes important for  $\omega_e \tau_e$  greater than unity. The values of  $\omega_e \tau_e$  over the range of initial shock tube densities, shock speeds and magnetic fields that are of interest range from about 0.2 to 0.7. Since continuous electrodes are used in the experiments,  $E_x = 0$ , and the effective electrical conductivity will be reduced by as much as 50 percent for  $\omega_e \tau_e = 0.7$ .

### (3) Ion Slip

The Lorentz Force is applied to the electrons since the current is almost entirely due to the electrons. The force is transmitted to the heavy ions by electrostatic fields which are generated by means of a slight charge separation. For the neutral particles to be accelerated, they must undergo sufficient collisions with the ions so that the momentum

increase of the ion stream is transmitted to the neutrals. The velocity of the ions, relative to the neutrals, is a measure of the "ion slip". It is shown in Reference 2 that in the absence of Hall currents the ratio of neutral velocity to ion velocity is given by:

$$\frac{V_{\text{neutral}}}{V_{\text{ion}}} = \frac{1}{1 + f (\omega_e \tau_e) (\omega_I \tau_{IN})} \quad (5)$$

where  $(\omega_I \tau_{IN})$  is the product of the ion cyclotron frequency and the ion mean free time for neutral collisions. The ion slip velocity becomes appreciable when  $f (\omega_e \tau_e) (\omega_I \tau_{IN}) > 1$ . Over the range of initial shock tube densities and shock speeds that are of interest in the experiments reported herein, the value of  $f (\omega_e \tau_e) (\omega_I \tau_{IN})$  is  $\ll 1$  and therefore no appreciable "ion slip" will occur.

#### (4) Electrode Loss

In the immediate neighborhood of the electrode surface there will be a voltage drop associated with the current flowing to the electrode. The electric power associated with this voltage drop and current will be converted into heat and dissipated in the electrode without substantially affecting the gas motion and must be considered a loss. The magnitude of this voltage drop is dependent on the electrode configuration as well as its temperature and composition through the manner in which these properties control the

boundary layer over the electrodes and the method of electron emission. Since the surface voltage drop is in series with the voltage across the electrode gap, the ratio of power lost at electrode surface to useful power is simply:

$$\frac{\Delta V}{uBh} \quad (6)$$

where  $\Delta V$  = electrode surface voltage drop, and  $h$  is the width of the electrode gap. Thus, in order that the power loss be small, the back emf of the accelerator must be large compared to the voltage surface drop.

In addition to having a reasonably low surface voltage drop, the electrodes must be capable to providing a uniform current density over their surface. In general, both of these requirements would indicate an electrode configuration which provides intimate contact between the gas and the electrodes by keeping the boundary layer as thin as possible. A variety of designs have been proposed to produce this desired effect, such as multiple points, wire mesh, or serrated electrodes<sup>(4,5,6,8)</sup>. In the experiments reported herein, no attempt was made to sophisticate the electrode design; they were simply copper strips. In these experiments the electrode loss was small under the conditions of maximum acceleration.

#### (5) Boundary Layer Losses

Along the surface of the electrodes the accelerating body force ( $\vec{J} \times \vec{B}$ ) is the same as in the free stream and

is of the same order as the viscous and inertia forces in the boundary layer. The body force has the same effect as a favorable pressure gradient and a normal aerodynamic boundary layer with its attendant momentum loss builds up on the electrodes. However, on the insulating walls of the accelerator (the walls normal to the magnetic field), the development of a viscous boundary layer has, in addition to the usual momentum loss, a second and possibly more serious effect; namely, this boundary layer provides a short-circuit path between the electrodes due to the fact that within this boundary layer (Hartmann type) the back emf is lower than in the free stream but the applied electric field ( $E_y$ ) is the same. Thus, near the wall currents as large as  $E_y$  can flow, and since these currents would be substantially greater than those in the free stream, large electrical losses could result.

In addition to the possible limitations mentioned so far, one fundamental limitation of this acceleration technique has been passed over; namely, that due to the finite diffusivity of the magnetic field. The principle of operation of the magnetohydrodynamic accelerator requires that the fluid enter and leave a region where an applied magnetic field exists. This is possible only if the time required for the field to leak into the fluid a certain characteristic distance is small compared to the time required for the fluid to flow the same distance; i.e., if the magnetic Reynolds number is small compared to unity. This ratio is given by:

$$R_m = \frac{\sigma}{\mu_0 u} \mathcal{L} \quad (7)$$

where  $\sigma$  is the gas conductivity,  $\mu_0$  is the permeability of free space,  $u$  is the fluid velocity, and  $\mathcal{L}$  is the characteristic length. At small values of  $R_m$  ( $R_m \ll 1$ ), Maxwell's equations are decoupled from the gas dynamic equations and the field should remain virtually unaffected by the fluid motion. In the experiments reported herein, the value of  $R_m$  at the entrance to the accelerator was about .5 based on the radius of the tube as a characteristic length. Since the conductivity as well as the velocity increases along the length of the accelerator, the original velocity may be increased by only a factor of two before the requirement of ( $R_m < 1$ ) is violated.

If, as the gas slug is accelerated,  $R_m$  becomes sufficiently greater than unity, then in order to leave the accelerator the gas must provide the energy needed to sweep out the magnetic field.

In the experiments to be reported two lengths of electrodes were used, 25 and 58 cms. respectively. The ideal length of test gas was about 70 cms and the measured length ( $l$ ) was about 15 cms. The electrical power supplied to the electrodes was varied from 0 to 11 megawatts. Table II shows representative values of significant parameters evaluated at the entrance of the acceleration for argon over the range of operation.

TABLE II

$B_o$ kg	Flow Mach $N_o$	$f$ $J_T = 25,000$ Amps	$\sigma$ mhos/cm	$R_m$ $= \sigma \mu_o u \pi$	$\omega_e \tau_e$	$\frac{\rho_2 V_S^2}{B^2 / 2 \mu_o}$	$\frac{\mathcal{L}}{= \frac{\sigma B^2 v}{\rho_2 u}}$
0	2.1	—	45	0.45	—	—	—
5	2.1	0.9	45	0.45	0.22	7.7	.2
15	2.1	0.3	45	0.45	0.67	0.8	2

## II. DESCRIPTION OF APPARATUS

The equipment used in the investigation may be conveniently grouped in the following way:

1. Shock Tube
2. Accelerator
3. Current source
4. Magnetic field source
5. Measuring devices

### 1. Shock Tube

The shock tube (see Figure 2) was a conventional combustion-driven tube of 1.5" inside diameter and 20 feet long. The driver consisted of a 2.5 foot length of 2.5" inside diameter pipe and was connected to the driven section through a reducing nozzle of two diameters in length. The driver was filled by first admitting oxygen at a pressure of 6.8 psig, then hydrogen was at 50 psig and finally helium at a pressure of 250 psig, the latter being used as a moderator to decrease the possibility of a detonation. The mixture was ignited by discharging a 20  $\mu$ f capacitor bank charged to 4000 volts through a .003" diameter copper wire which was stretched along the longitudinal axis of the driver. After combustion, the driver pressure was estimated to be about 1500 psi. A copper diaphragm (.023" thick), scribed in the conventional "X" pattern by means of a weighted glass cutter, separated the driver from the

driven section. The use of an oversize driver slightly increased the shock speed for a given driver gas pressure and temperature.

The driven section consisted of 16 feet of 1.5" inside diameter stainless steel pipe followed by the accelerator and a length of pyrex brand "doubld-tough" glass pipe. Two accelerators were used in these experiments: one 18" and the other 36" long. The shorter accelerator was followed by a three-foot section of glass pipe and the longer one by a two-foot section. A 15 cubic foot dump tank was connected to the end of the glass pipe to prevent a shock from being reflected into the tube. A .010" thick acetate paper diaphragm was used to isolate the dump tank from the driven section of the shock tube. Vacuum-tight joints in the shock tube were made with teflon gaskets and rubber "O" rings.

The driven section of the tube was pumped down by a mechanical vacuum pump. A liquid nitrogen cold trap was located between the pump and the shock tube. The lowest pressure to which the driven section could be pumped depended on whether the particular accelerator being used was made of glass or linen-base phenolic tubing. In the former case, the tube could be pumped down to somewhat less than 5 microns and it exhibited a combined leak and outgassing rate of one to two microns per minute over the first three minute interval after sealing the system. When the accelerator was constructed from phenolic tubing, the driven section could be pumped down to about 15 microns and under these conditions



the combined leak and outgassing rate was about 5 microns per minute during the first three minutes.

The driven section of the tube was filled by admitting the gas at the upstream end of the tube and exhausting it through the vacuum pump at the downstream end. This purging was continued for about five minutes before the system was sealed off. The shock tube was fired less than two minutes after the driven section was sealed off; thus the maximum amount of gas impurities due to leakage and outgassing was less than two percent for initial gas pressures of 2 mm. Hg.

## 2. Accelerator

Two different length accelerators were used in these experiments. The shorter one had a channel length of 18 inches, electrodes of 10" length and an applied magnetic field that extended over an axial distance of about 14". The longer accelerator had a channel length of 36 inches, 23" electrodes, and an applied magnetic field that extended over an axial distance of 29 inches. The length of the magnetic field cited here includes the 2" length at each end of the field over which the field decays to about 5 percent of its average value.

The accelerator was originally constructed of glass pipe, but the glass fractured violently when attempts were made to accelerate the gas by more than 50 percent of its original speed. As a result, the accelerator had to be constructed of thick-wall (1/4") linen base phenolic tubing.

The electrodes were made of .040" thick copper strips and were held tightly against the inside wall of the accelerator by machine screws soldered to the electrodes. The leads that carried the current from the capacitor bank to the electrodes were closely spaced copper strips that were bent into a cylindrical yoke at the end. This yoke was then fitted snugly against the outside wall of the accelerator at the upstream end. Two heavy brass screws, soldered to the yoke and the electrode, carried the current through the accelerator walls.

### 3. Current Source

The current was supplied by a 3600  $\mu$ f (2500 volt, 11,250 Joule) capacitor bank which was connected in series with the electrodes and an overdamping carbon resistor of high heat capacitance. With the electrodes short-circuited this overdamped RLC circuit reached its peak current in about 30 microseconds with an average current over this period equal to 75 percent of the peak, and the time for the current to decay to one-third of its peak value was about 600 microseconds. The capacitor bank was fired when the shock front had travelled to a station about 2.5" within the electrode gap. In this manner the current density in the gas remains nearly constant as the gas slug enters the electrode gap.

The firing of the capacitor bank was controlled by a 5551A Ignitron tube. The current pulse necessary to trigger

the ignitron was provided by a thyatron capacitor circuit whose grid bias was controlled by an ionization gage located 2.5" downstream from the leading edge of the electrode gap.

The highest total current that could be delivered to the accelerator by this equipment was about 25,000 amps.

#### 4. Magnetic Field Source

An air core single layer rectangular shaped coil was used to produce the applied magnetic field. The coil for the shorter accelerator measured approximately  $3\frac{1}{2}" \times 3\frac{1}{2}" \times 15"$  long. The coil was constructed out of 15 turns of No. 5 insulated square copper wire. The coil was formed in such a manner that the accelerator channel could be slipped through the small sides ( $3\frac{1}{2}" \times 3\frac{1}{2}"$ ) of the coil, the long sides of the coil being parallel to the shock tube axis. Thus the field generated by the coil was perpendicular to the gas flow.

The coil was connected in series with a 2400  $\mu\text{f}$  (2500 volts, 7500 Joule) capacitor bank and an ignitron, the latter being used as a switch to fire the bank at the appropriate time. The circuit rang at a measured frequency of 500 cps (or 500  $\mu\text{s}$  per one-quarter cycle). In order to allow the magnetic field to build up to its maximum value by the time the shock front reached the accelerator, the ignitron switch was closed about 500  $\mu\text{s}$  before the shock reached the accelerator. Thus, during the maximum testing

time of 100  $\mu$ s, the applied magnetic field varied by less than two percent. The current pulse required to trigger the ignitron (Model 5551A) was supplied by a thyatron-capacitor circuit, whose grid bias was controlled by an ionization gage located at an adjustable distance upstream from the accelerator.

At any given position along the longitudinal axis of the accelerator (i.e., the shock tube axis), the measured magnetic field for a fixed time did not vary by more than a few percent over the channel cross-section. Along the longitudinal axis of the accelerator, the measured magnetic field averaged over the tube cross-section had a maximum value at the mid-way point of the coil, then gradually decreased to 80 percent of the peak value at  $\pm 5.0$ " from the midpoint and then, near the ends of the coil, fell almost linearly to 5 percent of the peak value at  $\pm 7.0$ " from the midpoint.

The energy dissipated in this circuit by ohmic heating during the first one-half cycle was about 20 percent of the original energy stored in the capacitor bank.

The magnetic field coil for the longer accelerator was constructed in the same manner as the shorter one, and had the following characteristics:

Dimensions	3" x 3" x 30"
Number of turns	14; No. 5 square wire
Capacitor bank	4800 $\mu$ f, 2500 volts, 15,000 Joules

Measured ring frequency	270 cps
Measured magnetic field variation over channel cross section:	$\pm 3$ percent
Measured magnetic field along the longitudinal accelerator axis:	Peak at midpoint of the coil; 92 percent of peak at $\pm 12.5$ " from midpoint, 5 percent of peak at $\pm 14.5$ " from midpoint.
Variation of peak magnetic field over maximum testing times of 150 $\mu$ s:	$\pm 2$ percent
Measured $I^2R$ loss during first one-half cycle:	about 40 percent of initial energy in the capacitor bank.

## 5. Measuring Devices

The following quantities were measured for each run:

- A. Shock front velocity and flow behind the shock
- B. The electrical conductivity
- C. The current passed across the electrode gap
- D. The voltage drop across the electrode gap
- E. The initial pressure in the shock tube

### A. Shock Front Velocity

Two methods were used to measure the shock front velocity: (1) low voltage ionization gages, and (2) rotating mirror (smear) camera. The ionization gages consisted of a flange made from an electrical insulator through which two  $1/8$ " diameter brass rods,  $1/4$ " apart, were inserted and allowed to protrude about  $3/16$ " into the gas stream. The

two brass rods, a 24 volt auto battery, and a 4 ohm resistor were connected in series. When the shock front arrived at the ionization gage, the hot gases closed the gap between the rods, allowing a current to flow in the circuit. As a result, the voltage across the gap dropped rapidly (within 2  $\mu$ -seconds). In order to measure the shock front speed fore and aft of the accelerator, a pair of such ionization gages were located upstream of the accelerator and separated by a distance of five feet. A similar pair was located downstream of the accelerator and separated by a distance of 2 or 3 feet. The voltage signals from each pair of gages were recorded on a dual-beam oscilloscope, so that the time for the shock front to travel the distance between the gages could be easily measured.

A rotating mirror camera was used to obtain smear photographs of the shock-heated gases. In this technique, the camera was focused on either a vertical or horizontal slit of the tube and the image of the luminous gas was smeared out over a stationary film by means of a high-speed rotating mirror. The particular camera used in these experiments had a writing speed capability of several millimeters per microsecond.

When the camera was focused on a vertical slit, the smear photograph indicated the length of test gas and the uniformity of the radiation over the channel cross-section.

When the camera was focused on a sufficiently long horizontal slit, the smear photograph provided an accurate measure of the shock front velocity. It also provided a history of the length of the hot luminous gas slug, the uniformity of light output along the slug length, and in some cases it also provided a measure of particle velocity in the flow behind the shock front.

#### B. Electrical Conductivity

The method used to measure the electrical conductivity was the magnetic induction technique developed by Lin et al.<sup>(9)</sup>. In this technique, a field coil with its axis along the axis of the shock tube sets up an axially symmetric magnetic field with radial components. The moving gas interacts with this radial field causing a circumferential current to close within the gas. This ring current induces a magnetic field which links a search coil placed close to the field coil. The rate of change of this field with time due to the gas flow induces a voltage in the search coil circuit. This induced voltage is recorded as a function of time on an oscilloscope and from this response the gas conductivity may be calculated with the aid of a suitable calibration. The field coil had a resistance of 7 ohms and was connected in series with two 12 volt automobile batteries. The maximum axial field produced by this coil was calculated to be about 1300 gauss. This maximum field is approximately five times less

than that field strength at which the cyclotron frequency of the electrons in the gas is of the same order as the collision frequency of the electrons. This low field is required in order to prevent the electrons from being confined by the magnetic field. This gage was calibrated by shooting an aluminum slug through the coil and recording the response. The conductivity was found to be given by the relation.

$$\sigma = 11.7 \frac{a}{u} \text{ mho/cm} \quad (8)$$

where  $a$  is the area under the search coil response in millivolts times microseconds, and  $u$  is the gas particle velocity in meters per second.

#### C. The Current

The current flowing across the tube was measured by means of a search coil located between a set of flat parallel copper plates that served as part of the current leads. The output signal of this search coil was fed into an integrator in order to obtain a direct measure of the instantaneous current. The output of the integrator was compared (for capacitor bank voltages up to 600 volts) with the value of the current obtained by measuring the rate of change of the capacitor bank voltage with respect to time. With the available oscilloscopes, the latter measurements could not be made at bank voltages above 600 volts without the use of external attenuators, the characteristics of



which seemed uncertain under the experimental conditions.

The two measurements agreed with each other within  $\pm 5$  percent.

#### D. The Voltage Across the Electrodes

The voltage drop across the electrode gap was measured directly by means of a Tektronix oscilloscope equipped with a differential preamplifier. The oscilloscope leads were attached to the extreme downstream end of the electrodes in order that these leads would not link any of the magnetic flux produced by current flowing in the electrode circuit.

#### E. Initial Gas Pressure

The initial gas pressure in the driven section of the shock tube was measured by means of a Pirani gage. The Pirani gage was calibrated against a McLeod gage.

### III. DATA PRESENTATION AND DISCUSSION

The data is presented in the following order:

1. Experimental conditions
  - a. Shock tube flow
  - b. Range of experiments
2. Effects of circular geometry and open circuit voltage measurements
3. Shock attenuation due to aerodynamic drag and magnetic field
4. Voltage current characteristics
5. Evidence of acceleration
  - a. Measured increase in front speed
  - b. Measured increase in gas velocity, smear photographs
  - c. Time for test slug to travel through electrode gap
  - d. Time rate of change of induced electric field
6. Comparison of measured and predicted velocity increase, momentum balance
7. Energy conversion efficiency and energy balance
8. Electrical conductivity measurements
9. Generator experiments

#### 1. Experimental Conditions

##### A. Shock Tube Flow

The flow in the shock tube without the accelerator in operation is shown in the conventional x-t diagram in Figure 3. As the metal diaphragm separating the driver and driven section opens, a compression wave moves into the driven section and rapidly steepens to form a shock and an

expansion wave moves into the driver section. The gas behind the shock is heated and set into motion to the right. The "contact discontinuity" separating the driven gas from the driver gas broadens into a region where the two gases are mixed. This mixing results from turbulence associated with the opening of the heavy metal diaphragm and causes the actual length of pure hot argon test gas to be shorter than the ideal length expected from the x-t diagram.

In addition to this mixing phenomenon, at sufficiently low initial tube densities the boundary layer in the flow behind the shock front may impose an even more severe limit on the obtainable length of hot test gas (Reference 10). In the experiments reported herein, the actual slug length of test gas as determined from electrical conductivity and photomultiplier measurements remained approximately constant over the downstream half of the driven section and was equal to about  $1/4$  of the ideal length. It could not be discerned from the experimental results whether the boundary layer or the mixing at the "contact discontinuity" controlled the obtainable length of the test gas, and thus it was not clear whether the gas in all of region 2A of Figure 3 was a mixture of argon and driver gas (mostly helium) or whether it was simply cold argon.

The smear photographs showed that the length of luminous gas behind the shock front remained constant over

the full view field of the camera, about three feet of channel length. For the initial tube density at which most of the experiments were run, i.e,  $\rho_1 = 2$  mm. Hg., with argon as the working fluid, the length of luminous gas observed by means of the smear photographs was 15 cms. Over the same length of channel (3 feet), the ideal x-t diagram indicates that the shock accumulates enough new fluid to increase the slug length by an additional 10 cms. These observations are in agreement with others made in shock tubes operating at sufficiently low densities<sup>(10)</sup>.

The shocks utilized in these experiments to produce the hot flowing plasma were quite strong (about Mach 15). The gas velocity for a shock of this strength in argon is about 85 percent of the shock front velocity. The gas flow Mach number is slightly greater than 2, the gas temperature is about  $12,000^\circ\text{K}$ , and the static gas pressure behind the shock is about 1 atm., the degree of ionization being about 15 percent.

The flow in the shock tube with the accelerator in operation is shown in the x-t diagram of Figure 4. It should be noted here that the applied magnetic field, although sinusoidal in time, has a very long half cycle time ( $\sim 10^3 \mu\text{-sec.}$ ) and the applied magnetic field may thus be viewed as a d.c. field during the experimental time. The magnetic field coil is energized in sufficient time to allow the applied field to build up to its maximum value by the time the gas arrives

at the accelerator. It is assumed that the flow is not reflected as the shock enters the magnetic field, and so the flow remains essentially unaffected by the presence of the accelerator until the shock front arrives at station "b" (about 2.5" inside the electrode gap) at which time current flow across the electrode gap is initiated. The resulting  $\vec{J} \times \vec{B}$  body force accelerates the shock-heated gases and the shock front speed is correspondingly increased. Evidence that the flow is indeed accelerated was obtained from four measurements: (1) increase in shock front velocity as observed by means of the ionization gages and by means of the smear camera, (2) increase in gas velocity as observed by means of the smear camera, (3) time required for test slug to pass through the accelerator as measured from the gap voltage vs. time trace, and (4) increase in the induced electric field as the test slug is accelerated along the gap length as measured from the electrode voltage-time responses. At sufficiently high accelerations, the shock front velocity was observed to undergo a rapid reduction in velocity after it had travelled about ten channel diameters from the accelerator. Such an adjustment of the front speed would be expected as a result of the "new" fluid which the shock accumulates as it moves sufficiently far downstream and which must be brought up to a speed near  $V_s + \Delta V_s$ , and as a result of the fact that the gases far in back of the shock front were not pushed on with as strong a body force as the test gas.

In the horizontal smear photographs of experiments where the gas was accelerated, "streaks" resulting from patches of gas with high local luminosity were clearly visible in a region extending from about 15 cms to 80 cms behind the shock front. These streaks provide a measure of the gas velocity and from these measurements (when made in the vicinity of station "d", the entrance to the glass channel) it was seen that substantial acceleration was produced in the gas up to a distance of about 60 cms behind the shock front. The experimental evidence indicated that not only the test slug (Region 2) was accelerated, but that the originally non-luminous gases in Region 2A became luminous and were accelerated to approximately the same velocity as the gases in Region 2.

A representative sketch of the current and voltage vs. time responses is also shown in Figure 4.

The current vs. time and voltage vs. time traces were portrayed on a dual beam oscilloscope to facilitate comparison. The voltage traces showed three distinct jumps in the voltage drop across the electrode gap. The first jump was completed in about one  $\mu$ sec., and took place as the shock front entered the electrode gap, and represents the induced back emf. The second jump was completed a few  $\mu$ -sec. and occurred when the applied current started to flow. After the second jump, the voltage continued to increase at a rate approximately proportional to the magnitude of the applied

body force and the applied magnetic field. The third observed jump took place over a much longer time interval (15 to 35  $\mu$ -sec.) than the first two and constituted a two- to four-fold increase in the voltage drop across the electrodes. This third increase was taken as evidence that the test gas slug was leaving the electrode gap and being followed by a mixture of driver gas and argon with much lower electrical conductivity. In general, after the third jump the voltage remained at about the same level for a few hundred microseconds.

The current vs. time responses show that after the electrode-capacitor bank circuit is closed, the current builds up from zero to a peak value in about 30  $\mu$ -sec. In an additional 50  $\mu$ -sec., the current has decreased to about 75 percent of its peak value. The current then remains at about 75 percent of its peak value until it cuts off after a total interval of about 110 to 250  $\mu$ -sec., depending upon whether the particular run was in the low or high current range. This latter dependence of the current duration stems from the fact that in general the current was adjusted by changing the voltage to which the capacitor bank was initially charged, with the result that at low applied currents (low bank voltage) the circuit was unable to maintain a constant current after the multiple voltage jump that takes place as the hot slug leaves the electrode gap. It should be pointed out that it took about 250  $\mu$ -sec. for the "ideal" slug length of argon

to travel through the electrode gap and that the argon was followed by driver gas which, being almost all helium, was not electrically conducting.

#### B. Range of Experiments

Two groups of experiments were performed; one using the shorter accelerator (10" electrodes), and one using the longer accelerator (23" electrodes). In the former group of experiments, the shock tube was first operated using argon as the working fluid at a fixed initial density of 2 mm. Hg. and a shock speed of Mach 15 while the applied magnetic field was varied from 0 to 15,000 gauss in steps of 5,000 gauss. The applied magnetic field was then held constant at 10,000 gauss and the initial tube density was first reduced to 1 mm. Hg. and then increased to 3 mm. Hg. Finally, air was substituted for argon as the working fluid, and a set of experiments was run with an initial shock tube density of 2 mm. Hg. and an applied magnetic field of 10,000 gauss. In most of the sets of experiments, the total applied current was varied from 0 to 25,000 amps.

In the second group of experiments, those using the long accelerator, the initial shock tube density was held constant at 2 mm. Hg. and the applied magnetic field was held fixed at 10,000 gauss for the first set of experiments in argon, and at 15,000 gauss for the second set. Finally, air was substituted for argon as the working fluid and one run was made with an applied field of 10,000 gauss.



In addition to the acceleration test, a few experiments were made with the electrode leads of the short accelerator disconnected from the current source (capacitor bank) and connected through a resistance load. Electrical power was thus tapped out of the device and dissipated in the external load.

Table III shows some of the parameters of interest at the entrance and exit of the accelerator for each of the various sets of experiments.

## 2. Channel Geometry and Open Circuit Voltage Measurements

Before discussing the results of the accelerator experiments, some consideration must be given to the circular geometry of the accelerator channel. Fishman<sup>(11)</sup> has made an analytical study of the circular geometry compared to the rectangular geometry of the same cross-sectional area and flow parameter. This analysis assumes (1) a long channel with both the magnetic Reynolds number and the interaction parameter ( $\sigma r B^2 / \rho u$ ) based on the channel radius much smaller than unity, and (2) that the electrical conductivity is a scalar quantity. These assumptions imply that none of the flow parameters change significantly in one tube radius; that the fluid velocity is along the channel axis only, and is of constant magnitude; and the only magnetic field is the applied field. In this study, Fishman showed that the behavior of the steady magnetohydrodynamic flow through the

# Short Accelerator

	B	kG	OPERATING CONDITIONS	
	P <sub>i</sub>	mm Hg		
	Flow Mach No.			
	Shock Mach No.			
	V <sub>s</sub>	m/sec		
	R <sub>m</sub> = σμ <sub>0</sub> uπ		ACCELERATOR ENTRANCE	
	P <sub>2</sub> V <sub>s</sub> <sup>2</sup> /B <sub>0</sub> <sup>2</sup> /2μ <sub>0</sub>			
	w <sub>e</sub> τ <sub>e</sub>			
	f at J= 25,000 amps			
	Measured slug length cm.			
	Ave.	V <sub>s</sub> +ΔV <sub>s</sub> m/sec	ACCELERATOR EXIT (Max. J run)	
	Peak			
	P <sub>2</sub> (V <sub>s</sub> +ΔV <sub>s</sub> ) <sup>2</sup> /B <sub>0</sub> <sup>2</sup> /2μ <sub>0</sub>			
	r			
	R <sub>m</sub> = σμ <sub>0</sub> uπ			
	φ/u B <sub>0</sub> h			

not measured

## OPERATING RANGE FOR ARGON EXPERIMENTS

TABLE III

circular channel depends upon the width of the electrodes. The narrow electrodes make poor contact with the fluid, thus giving the channel a high internal resistance, whereas wide electrodes are in part parallel to the induced and applied electric field and hence cause eddy current losses. These eddy currents flow between the edges and center of each electrode independently. It is to be noted that the power dissipated in these eddy currents is a source of entropy which does not vanish with vanishing current flow in the external circuit. The optimum electrode width depends on the desired performance characteristic. Fishman showed that for the case where the channel was to be used as a generator and maximum power was to be tapped off, the electrode width should be such that each one subtends an angle of  $\alpha = 80^\circ$  with the tube axis. If a channel efficiency of 80 percent is desired, then an angle of  $\alpha = 60$  percent permits an output power about 12 percent less than the rectangular channel of the same efficiency. If the channel is loaded to give the same power as an 85 percent efficient rectangular channel, it will have an efficiency of 82 percent. The electrodes used in the experiments reported herein had a value of  $\alpha = 65^\circ$ . From the analytical study, this value of  $\alpha$  gives a value of the parameter  $\sigma R_g$  equal to 1.2 and  $(\phi)_{o.c.}/u r B_0 = .91$  where  $R_g$  is the resistivity of the gas,  $\phi_{o.c.}$  is the open circuit voltage across the electrodes,  $u$  is the gas velocity, and  $r$

is the tube radius. The former indicates the relative increase in channel electrical resistance compared to a square channel with full-width electrodes. The latter parameter is the relative decrease in the electrode spacing due to the circular geometry; that is,  $(\phi)_{o.c.}/uB_0$  may be taken as an effective separation distance of the electrodes.

The assumptions on which Fishman's study was based will, of course, in general not be satisfied in the case of high acceleration experiments. However, they will be satisfied for experiments where the external electrode circuit was open circuited. Representative open circuit voltage vs. time traces are shown in Figure 5 for the case of  $B_0 = 5, 10, \text{ and } 15$  kilogauss. From these voltage traces it is seen that as the front of the gas slug moves into the electrode gap, the voltage increases. This increase approximately follows the shape of the applied magnetic field along the accelerator axis, but the voltage level is some 5 percent lower than the local value of  $uB_0$ . This latter discrepancy appears to be due to end effects. During the time interval that the test slug is entirely within the electrode gap, the measured voltage is at its peak value and the local value of  $B_0$  is also at its peak and equal to 5, 10, and 15 kilogauss. These peak values are plotted in Figure 6. Over a range in magnetic field strength of 5 to 15 kilogauss and a gas velocity range of 3200 to 4100 m/sec., the measured open

circuit voltages are a few percent less than the predicted values ( $= .91 \mu B_0 2r$ ) which implies that other internal short circuit paths are not substantial under these conditions but do exist. The presence of a Hartmann boundary layer on the non-conducting walls provides a possible short circuit path.

For the case of such an MHD boundary layer growth over a flat insulating plate, Moffatt<sup>(12)</sup> points out that at the beginning of the plate an equilibrium exists between the viscous and inertial forces, the magnetic force not being significant; whereas at a distance of one interaction length ( $l_{b.l.} = \mu/\sigma B^2$ ) or more, the magnetic forces and viscous forces establish an equilibrium with the inertial forces becoming relatively unimportant. Thus the MHD boundary layer should be established in a distance  $l_{b.l.}$  from the leading edge of the electrodes. For both the hot and cold wall cases considered by Moffatt, the thickness of the MHD boundary layer was calculated to be of the order of the Hartmann thickness ( $\delta_H = \sqrt{\frac{\mu}{\sigma B^2}}$ ). For the experiments presented here, the values of the interaction lengths are 12.7, 3.2, and 1.4 cms. for  $B_0 = 5, 10, \text{ and } 15$  kilogauss, respectively for argon of  $\rho_1 = 2$  mm Hg.

If the MHD boundary layer is assumed to be of uniform thickness equal to the Hartmann thickness ( $\delta_H$ ) along the length of the electrodes, and if the conductivity of the gases in this layer is assumed to be equal to that of the gases

in the free stream, and if a linear velocity profile is assumed then the current flowing through the MHD boundary layer when the electrodes are open circuited may be calculated and the resulting decrease in open circuit voltage determined. This reduction in  $\phi_{o.c.}$  is of the order of a few volts and is shown as curve "B" in Figure 6. Since the scatter in the data is of the same order as the difference between curves "A" and "B" it can only be stated that the order of magnitude of the short circuit currents flowing through the MHD boundary layer is given by assuming this layer to be of constant thickness  $\delta_H$  and to have an electrical conductivity equal to that of the free stream gases (the value of viscosity used to calculate  $\delta_H$  was taken from Reference 15). It should be pointed out that these internal short circuit currents close completely within the gas.

Only the component of  $\vec{J}$  perpendicular to the magnetic field is effective in producing an axial acceleration of the gas. Thus, to calculate the ideal body force, the space average value of this component of the current must be determined. However, this averaging appears to depend on the channel loading and is not readily computed. As a result, and as a first approximation based on Figure 6, the calculations made in the following discussion assume (1) that the circular channel can be treated as if it were a rectangular channel of the same cross-sectional area with full width

electrodes which are separated by a distance of  $h = .91(2r) = 3.48 \times 10^{-4}$  meters, and (2) the internal gas resistivity is  $1.2/\sigma$ .

### 3. Shock Speed Attenuation due to Aerodynamic Drag and Applied Magnetic Field

In order to determine the effects of the aerodynamic drag and the applied magnetic field on the flow downstream of the accelerator, experiments were performed in which no current was supplied to the accelerator but the applied magnetic field was varied from zero to 15 kilogauss.

The measured values of the shock speed attenuation for the case of the short accelerator using argon at an initial tube density of 1 and 2 mm. Hg. and a shock Mach number of 15 and 17 are shown in Figure 7 and 8 respectively. These measurements are based on the average upstream and downstream front velocity as measured by means of the ionization gages and thus represent the attenuation over 5.5 feet of channel.

When the measurements for the case of an initial tube density equal to 1 mm. Hg. were made, the electrodes were removed from the channel, whereas the measurements for the case with  $\rho_1 = 2$  mm. Hg. were made with the electrodes in place. In the latter case, the curved electrodes provided a source of entropy even though the electrodes were not connected to an external load.

The attenuation due to the aerodynamic drag only is seen to be of the order of 10 percent or about 1.8 percent

per foot of channel. The additional attenuation due to the presence of the magnetic field (short accelerator) is of the order of 5 percent at the maximum applied field. When the values of attenuation for the two initial densities are compared at a given value of the ratio of magnetic pressure to gas pressure, the absence or presence of electrodes seems to make little difference.

For the experiments where the electrodes were present ( $\rho_1 = 2$  mm. Hg.), the electrical conductivity was measured at a station about 15 diameters downstream from the electrodes. A representative sample of the conductivity gage responses is shown in Figure 9. From the responses, it is seen that at sufficiently high magnetic fields ( $> 7.5$  kilogauss) the conductivity no longer remains constant over the slug length but rather goes through a slight decrease and then a larger increase so that the gas in the rear of the slug has a higher conductivity than the gas in the front portion of the slug. It is to be noted from Figure 9 that a similar distortion is observed when  $B_0 = 0$ , but the conductivity measurement is made further downstream, about 24 diameters from the electrodes. This same type of distortion of the conductivity profile of the slug was also observed in the generator experiments and even more severely in the accelerator experiments when a current, but no magnetic field, was applied. Smear photographs taken under the latter conditions



showed that the region of lowered conductivity was also a region of lowered luminosity.

#### 4. Current, Voltage Characteristics

Figure 10 shows the measured current-voltage characteristics when there was no externally applied magnetic field. At sufficiently high currents, the back emf increases as the slug moves down the electrode gap. This results from the "backstrapping" effect brought about by the manner in which the current is carried to the gas slug. In Figure 10, the lower points represent the voltage drop across the gap near the entrance of the accelerator and the high points represent the voltage near the exit.

Curve "A" in Figure 10 represents the voltage required to drive a given current across the tube assuming no electrode voltage drop, that the conductivity remains equal to the measured upstream value, and that the gas slug is entirely within the electrode gap. Curve "B" is based on the same assumptions as "A" except that the conductivity is taken as the arithmetic mean of the measured upstream and downstream values. Thus, the difference in voltage between the experimental curve and curve "B" may be taken as a measure of the total voltage drop associated with the electronic processes taking place within the boundary layers. This potential drop decreases from about 55 volts at  $J = 3000$  amps to about 44 volts at  $J = 24,000$  amps.

Assuming uniform current density at the electrode surface, the range of total current  $J_T = 3000$  to 24,000 amps corresponds to a current density range of  $10^2$  to about  $10^3$  amps/cm<sup>2</sup> when the slug is entirely within the electrode gap.

## 5. Evidence of Acceleration

### A. Measured Increase in Downstream Front Velocity

Figures 11 and 12 show the measured fractional increase in shock front velocity  $\left(\frac{V_s + \Delta V_s}{V_s}\right)$  for the group of experiments where the working fluid was argon at an initial tube density of 2 mm. Hg. The curves are fitted through the experimental points. Not all the experimental points are shown. When the curve for a given applied magnetic field has two branches, the lower one represents the downstream velocity averaged over the length of glass pipe following the accelerator as measured by the ionization gages. The upper curve represents the highest velocity observed near the entrance to the downstream glass pipe section. This peak velocity was measured by means of the rotating mirror camera. In those experiments for which the shock front velocity was observed to be constant over the length of the glass pipe, the simultaneous speed measurements made by means of the ionization gages and by means of the smear camera agreed within  $\pm 3$  percent.

The vertical bars represent experiments in which smear photographs indicated a change in front speed in the

channel downstream of the accelerator. The observed change in front velocity occurred very rapidly, the adjustment being completed in about one tube diameter of travel, or in a few  $\mu$ -sec. In some cases the speed reduction took place in one step, whereas in other cases the adjustment took place in two steps. The distance from the trailing edge of the electrodes to the point at which the adjustment occurred varied from about 7 to 14 channel diameters.

In Figures 11 and 12 lines have been drawn to indicate the total current for each value of applied magnetic field for which the magnetic Reynolds number at the exit of the accelerator becomes equal to the stated values. The value of the channel loading parameter ( $K = \phi / u B_0 h$ ) evaluated at the exit of the accelerator is also shown for the experiments of maximum applied current.

It should be noted that the observed velocity increase in the set of experiments in which no externally applied magnetic field was used stems from two effects: first, the compressibility effects of the flow behind the shock front, and second, the "backstrapping;" that is, the body force resulting from the interaction of the applied current and the magnetic field that is generated by the same current flowing along the length of the electrodes. The strength of this magnetic field increases with the total applied current and has an average value less than 1500 gauss at the maximum applied current of 25,000 amps. The combined

compressibility and backstrapping effects result in a downstream front velocity equal to 1.35 times the upstream value for the case of maximum applied current. In the calculations that follow, the magnetic field is assumed to be equal to the externally applied magnetic field,  $B_0$ , and does not include the magnetic field that results from the "backstrapping".

The remaining velocity data; that is, the results for the air experiments and for argon experiments at initial tube densities of 1 and 3 mm. Hg., are shown in Figure 13.

The argon experiments are discussed in some detail in the following pages whereas the air experiments, being somewhat less "clean" are presented here only to demonstrate the feasibility of this acceleration technique in another working fluid. The lack of clarity in the air experiments stems from the fact that the chemical composition of the air admitted to the shock tube was not controlled and much more of the electrical power is consumed at the entrance to the accelerator in heating the fluid than in accelerating it ( $f = 7$ ).

Since the slug lengths and molecular weights are about equal for air and argon, one would expect the increase in velocity of the two gases to be about the same for the same values of  $B_0$ ,  $J$ , and  $\rho_2$ . From Figures 11 and 13 this is seen to be approximately the case; the increase in shock front velocity for air being slightly less than that for argon at low currents and slightly more at high currents.

### B. Smear Photographs

Both vertical slit and horizontal slit smear photographs were taken downstream of the accelerator. The vertical pictures for the experiments in which the accelerator was not in operation showed the shock front to be normal to the tube axis, and that the luminosity boundary separating Regions 2 and 2A of Figure 4 extended over a channel length equal to a tube diameter. When the accelerator was in operation, the vertical smear photographs showed the gas in Region 2A to have become luminous, although the luminosity in this region was not uniform over the tube cross-section, the core of the flow being considerably more luminous than the outer layers at lower values of applied current, while the reverse was found to be the case at high currents. Furthermore, for the experiments where appreciable acceleration was produced, ( $\Delta V_s > 1/2V_s$ ), the shock front was distorted (see Figure 24B).

The horizontal smear photographs for the case where the accelerator was not in operation showed the length of luminous gas and front speed to remain constant over the full field of view of the camera, about 3 feet. In those experiments where the accelerator was in operation, the horizontal smear pictures indicated that the gas in Region 2A had been accelerated to about the same velocity as the gas in Region 2. The smear photographs are presented in

more detail in Appendix A. A brief summary of the shock front and gas velocities is given in Table IV for the experiments using argon at an initial pressure of 2 mm. Hg.

TABLE IV  
SUMMARY OF SMEAR PHOTOGRAPH VELOCITY MEASUREMENTS

$B_o$	$J_T$	$V_s + \Delta V_s$		Gas velocity $u_x$ at a Distance $x$ behind shock (Measured at Station d)			Distance behind shock at which $u$ =upstream value (Measured at Station d) cms
		Peak	Ave	$u_x$ m/sec.	$x$ cms	$\frac{u_x}{(V_s + \Delta V_s)_{ave}}$	
kg	amps	m/sec.	m/sec.	m/sec.			
0	0	4250	4250	3600	--	.85	--
5	7700	5000	5000	4500	50	.90	60
5	20700	6450	6450	5740	55	.89	120
10	6300	5860	5860	4800	35	.82	60
10	17800	8300	7800	6400	45	.82	100
10	4760	6250	5700	4720	30	.83	50
15	13330	11600	7550	7250	45	.97	100

It should be pointed out here that after the test slug gas (Region 2) passed through the accelerator, the applied current continued to flow across the electrode gap by passing through the cooler gas in Region 2A. When the expanded combustion driver gases filled the gap,\* the current flow was extinguished since the driver gases, being mostly helium, are not electrically conducting under these conditions. The smear photographs indicate that the gas velocity decreases to its original upstream value in the vicinity of the contact discontinuity.

\*It is to be noted from Table IV that when the applied current was low, the length of gas behind the shock front that was accelerated was not as long as the corresponding length when the applied current was high. This is apparently due to the fact that at low values of  $J$ , the current is observed to flow for a shorter time interval than for the case when  $J$  is high due to the fact that the current is controlled by the initial bank voltage, as was previously pointed out.

### C. Time Required for Test Slug to Travel Through Accelerator

With the particular experimental arrangement used in these tests, all sections of the slug of test gas will tend to move at the same instantaneous velocity. The reason for this becomes evident if it is assumed, for instance, that during the early part of the acceleration period, the front of the slug is accelerated to a velocity greater than the remainder of the slug. The back emf must then become greater in the front section of the slug with a subsequent decrease in the current density in that region. Since the total current supplied to the accelerator is constant, the lower current density in the front portion of the slug must be accompanied by an increased current density in the remainder of the slug which results in larger local accelerating forces. Thus, the induced voltage tends to maintain the current density in a manner which leads to uniform axial velocities along the slug length. In this manner, the slug should tend to "stay together" as it is accelerated.

Figure 14 is a plot of the time interval ( $t_m$ ) that the slug remains in the electrode gap as measured from the voltage traces vs. the time ( $t$ ) required to travel the same distance if the slug had an average velocity equal to the mean of the measured upstream and downstream velocity, namely,

$$(t) = \frac{L + \ell}{V_s + \frac{\Delta V_{sp}}{2}} \quad (9)$$

where  $L$  is the length of the electrode from the station at which the applied current is turned on to the downstream end of the electrode ( $L = 7.4''$  for the short accelerator;  $19.8''$  for the long accelerator),  $l$  is the axial length of the test slug at the entrance to the accelerator, and  $\Delta V_{sp}$  is the velocity increase based on maximum downstream front velocity observed by means of the smear camera.\*

The experimental points fall close to the  $45^\circ$  line which, together with the assumption that the slug length remains essentially constant as it passes down the accelerator, implies that the average velocity of the slug while in the accelerator is approximately equal to the arithmetic mean of the measured velocity upstream and downstream of the accelerator.

#### D. Measurement of the Time Rate of Change of the Voltage Across the Electrodes

The measured voltage drop across the electrode gap is due to three effects; the voltage required to drive the current across the test gas ( $J_s R_g$ ), the induced back emf ( $u B_0 h$ ), and the voltage drop associated with the electronic processes occurring within the boundary layer ( $\Delta w$ ).

\*In the smear photographs the shock front does not become visible until the shock has travelled about four tube diameters from the downstream end of the electrodes.



Thus the voltage drop across the slug may be expressed as:

$$\phi = J_s \cdot R_g + uB_o h + \Delta v \quad (10)$$

and the change of voltage with time may be expressed as:

$$\frac{\partial \phi}{\partial t} = J_s \frac{\partial R_g}{\partial t} + R_g \frac{\partial J_s}{\partial t} + B_o h \frac{\partial u}{\partial t} + \frac{\partial \Delta v}{\partial t} \quad (11)$$

Of the four terms on the right-hand side of the last equation, the first will be negative as the slug enters the gap since the area across which current can flow is increasing and continues to be negative when the test gas is entirely within the gap due to the fact that the gas conductivity is increasing as a result of ohmic heating. The first term finally becomes positive as the test gas leaves the electrode gap. The second term is positive for about the first 35  $\mu$ -sec. of current flow, and is negative afterwards as may be seen from the typical current trace of Figure 4. The fourth term is seen to be approximately zero from Figure 10 in the case of the short accelerator for all values of  $J_s$  and one would expect the same to hold true for the long accelerator, and thus the fourth term may be neglected compared to the other three terms. The relative importance of the first three terms of the equation are shown in Table V for a few values of  $J_s$ ,  $B_o$ , and the time elapsed from the beginning of current flow ( $t_j$ ) where  $\frac{\partial u}{\partial t}$  is assumed equal to  $.85 \frac{\Delta V_s}{t_m}$ .

TABLE V

RELATIVE MAGNITUDE OF TERMS

$B_o$	$J_s$	$J_s \frac{\partial R}{\partial t} / B_o h \frac{\partial u}{\partial t}$			$R_g \frac{\partial J_s}{\partial t} / B_o h \frac{\partial u}{\partial t}$		
		$t_J=10\mu s$	$t_J=35$	$t_J=45$	$t_J=10\mu s$	$t_J=35$	$t_J=45$
5	15,000	-1.5	0	0	+ 3.4	0	- 0.2
10	15,000	-0.2	0	+ .2	+ 0.4	0	- 0.05

Since, from the data, it is difficult to discern an accurate value of  $\partial\phi/\partial t$  over a time interval shorter than about 25  $\mu$ -sec., the experimental verification of the manner in which the voltage across the gap changes with the velocity of the test slug is not accurately possible due to the influence of first and second terms of Equation (11). A plot of the average measured values of these two quantities showed that  $\frac{\partial\phi}{\partial t}$  at low values of  $B_o$  was almost twice as large as  $B_o h \frac{\partial u}{\partial t}$  and equal to or slightly larger than  $B_o h \frac{\partial u}{\partial t}$  at high values of  $B_o$ , a trend that would be expected from the comparisons shown in Table V.

6. Comparison of Predicted and Measured Velocity Increase, Momentum Balance

If the test gas is assumed to be represented by a simple slug model where the mass (M) remains constant and

equal to  $\rho u A l$  as measured upstream of the accelerator and is acted on by a body force,  $J B_0 h$ , for a time interval  $t_m$  equal to the measured time interval from the initiation of current flow until the tail of slug leaves the accelerator, then the total change in the gas velocity is given by:

$$\Delta u = \frac{J B_0 h t_m}{M} \quad (12)$$

If the gas velocity is assumed to be 0.85 times the shock front velocity as previously discussed, then Equation (12) may be expressed as

$$.85 \Delta V_s \sim \frac{J B_0 h t_m}{M} \quad (13)$$

The experimental values of Equation (13) are plotted in Figure 15. The measured change in shock front speed used in this figure is the peak change observed by means of the smear camera; that is, it corresponds to the downstream shock front velocity over approximately the first 10 channel diameters downstream of the accelerator. Curve A is based on the assumption that all of the current supplies to the accelerator during the time interval ( $t_m$ ) goes through the test gas (Region 2). Curves B and C correspond to the short and long accelerator, respectively, and are based on the assumption that the total current supplied to the accelerator during the time interval ( $t_m$ ) divides, part going through the test slug, and the other part going through

the gases behind the test slug (Region 2A). Furthermore, it is assumed that the gases in both Region 2 and 2A pass through the accelerator at about the same speed and that the total current divides as it would for two resistors in parallel. The relative average resistance of the gases in Regions 2 and 2A were estimated from the measured voltage and current vs. time responses. Thus, the current that passes across the gap by going through the test slug is given by the expression:

$$J_s = \frac{J_T}{1 + R_{g2}/R_{g2A}} = \frac{J_T}{1.29} \text{ for short accelerator} \quad (14)$$

$$= \frac{J_T}{1.55} \text{ for long accelerator}$$

where  $J_T$  is the total current supplied to the electrodes, and  $R_{g2}$  and  $R_{g2A}$  are the resistivities of the gas in Region 2 and 2A, respectively.

To compensate for the aerodynamic and magnetic drag (that is, the attenuation observed when no current is applied), the predicted curves in Figure 15 are drawn not through the origin but rather through the experimental ordinate intercept. Drawing the curves in this manner implies that the total attenuation through the machine due to the aerodynamic drag and magnetic field is always represented by a constant drop in velocity (about 500 m/sec.) independent of the magnitude of the acceleration. From Figure 15 it is seen, for

the case of the short accelerator, that the experimental points follow the trend of curves B but fall slightly below the curve except for the experiments conducted with the lowest applied magnetic field. For these experiments, the "backstrapping" effect at high currents augments the applied body force with the result that these points fall above those for experiments conducted at larger values of the applied magnetic field. For the case of the long accelerator Figure 15 shows the experimental points to lie close to curve C.

It is known from shock tube experiments<sup>(10)</sup> and can be easily seen from the smear photographs presented in Appendix A, that as the shock travels downstream, the luminous test slug remains about constant in length and attenuates about 5 percent in speed over a channel length in which a mass of "new" fluid equal to that of the test slug is accumulated by the shock. The momentum imparted to this accumulated mass must then be delivered by the push of the driver gas and the slug length remains constant due to the fact that the "new" luminous fluid is accumulated at the same rate as moving luminous fluid is lost to the tube walls. In the case where the test gas is substantially accelerated it is not clear whether the excess momentum ( $\Delta M \Delta u$ ) over that normally imparted in the absence of the accelerator ( $u \Delta M$ ) to the "new" fluid accumulated by the shock as it moves through the accelerator is imparted by means of the driver

gas pushing or by the MHD body force. In order to judge which of the two is the source of the excess momentum, the measured values of  $\Delta u$  are plotted in Figure 16 against the calculated  $\Delta u$  for the test slug with a current  $J_s$  and a magnetic field  $B_o$ . The predicted curves are again drawn through the ordinate intercept to compensate for the aerodynamic and magnetic drag. Curve A is based on the assumption that the MHD body force due to  $J_s$  and  $B_o$  accelerates from  $u$  to  $u + \Delta u$  only a mass  $M$  equal to upstream slug mass, whereas for Curves B and C the mass is taken equal to the original slug mass  $M$  plus the mass ( $\Delta M$ ) accumulated in the short and long accelerator respectively. From Figure 16 it is seen that the experimental points in general fall closer to curve A than to B or C, indicating that the gases in back of the test slug provide the source of additional momentum to the accumulated fluid and thus the MHD body force associated with the current flowing in the test slug ( $J_s$ ) appears to be accelerating a fixed mass,  $M$ .

The ratio of the measured increase in gas velocity to the ideal increase is a measure of the accelerator's ability to impart momentum to the gas flow and may be spoken of as the "momentum efficiency". It is not clear whether the "ideal"  $\Delta u$  for the test gas should be based on all the current supplied to the machine ( $\Delta u = \frac{J_T B_o h t_m}{M}$ ) or whether it should be based only on the current that passes through

the test gas ( $\Delta u = \frac{J_{s o m} B t}{M}$ ). Both of these criteria imply that the mass of the test gas remains constant and that both the momentum ( $u \Delta M$ ) as well as the excess momentum ( $\Delta u \Delta M$ ) is imparted to the test slug by the push of the gases that follow. However, the former criterion implies that in the absence of current flowing through the gases in Region 2A, the gases behind the test slug could not supply all of the momentum to the "new" fluid, therefore, on the basis of this criterion, the sum of the currents through Region 2A and 2 must be charged to accelerating a slug of constant mass M and the "momentum efficiency" is about 70 percent for the short accelerator, and about 60 percent for the long accelerator. Based on the latter criterion, the momentum efficiency of the accelerator is about 90 percent.

In order to determine clearly the momentum efficiency of the accelerator the ambiguity introduced by the current dividing between Region 2 and 2A must be removed and furthermore, sufficient test gas must be provided to establish steady flow. Experimentally this requires a test slug length which is long compared to the diameter and electrode length. It was not possible to meet these requirements with the existing equipment and at the same time produce substantial acceleration.

Since the smear camera results showed the gases in Region 2A as well as those in Region 2 to be substantially

accelerated, it is interesting to compare the measured increase in velocity to what would be expected for a steady state flow device. Here it is assumed that the magnetic field is constant over the accelerator length and that the voltage drop across the gap is also constant along the length of the electrodes. Thus, at the entrance to the accelerator, the current density is high and the induced electric field is low, whereas at the exit the current density has decreased to zero and the induced electric field has increased so as to equal the applied field. Writing the conservation equations for the model, with argon as the working fluid, between the accelerator entrance (1) and exit (2) gives:

$$\text{Mass: } \rho_1 u_1 = \rho_2 u_2 = G \quad (15)$$

$$\text{Momentum} = \rho_1 + \rho_1 u_1^2 + \frac{\int (\vec{J} \times \vec{B}) dv}{A} = \rho_2 + \rho_2 u_2^2 \quad (16)$$

The equation of state and expression for enthalpy are:

$$\text{State: } P = \rho (1 + \alpha) R_o T \quad (17)$$

$$\text{Enthalpy: } H = \frac{5}{2} (1 + \alpha) R_o T + \alpha \frac{q_o}{m_o} \quad (18)$$

where:  $q_o$  = ionization potential per atom

$m_o$  = mass per atom of original gas

These together with the expression for the percent ionization which may be obtained from the law of mass action assuming thermodynamic equilibrium



$$\alpha = [2.54 \times 10^5 \frac{P}{T^{5/2}} \exp (\frac{1.821 \times 10^5}{T}) + 1]^{-\frac{1}{2}} \quad (19)$$

where: T = temperature °K

P = pressure in atoms.

form a set of six equations in six unknowns from which the increase in velocity may be determined as a function of the parameter,  $\frac{JB_o h}{\dot{m}}$ . Figure 17 shows a plot of the measured increase in speed ( $\Delta u = 0.85 \Delta V_{sp}$ ) as a function of the above parameter. Since this parameter is about the same as the expression for the velocity increase based on the simple slug model for the case of the short accelerator ( $JB_o h / M/t_m$ ) one would expect the experimental points to lie close to the predicted curve which is seen to be the case from Figure 17. For the long accelerator  $M/t_m$  is appreciably smaller than  $\dot{m}$  and the experimental points fall above the predicted curve. It should be noted here that the density used in the steady state flow calculation was the density of the gases in Region 2, whereas the density of the gases in Region 2A is uncertain and depends on the unknown values of the temperature and composition of the gas; that is, whether the gas is cold argon or a mixture of argon and driver gas.

## 7. Energy Conversion Efficiency and Energy Balance

The ratio of the increase in kinetic energy ( $\Delta KE$ ) of the test gas slug to the electrical energy input ( $J \cdot \phi t_m$ ) may be taken as a measure of the energy conversion efficiency

of the device. Again as in the case of determining the momentum efficiency, the question arises as to whether the total electrical energy delivered to the electrodes during the time interval ( $t_m$ ) should be charged to accelerating the flow or whether only that part of the energy associated with the current passing through the gas in Region 2 should be used. The energy conversion efficiency based on each of these two criteria is plotted in Figure 18 against the rate of electrical energy input. The total input power range is from 0.5 to 11 megawatts. Over all but the lower end of this power range, the energy conversion efficiency is of the order of 40 percent when based on the former criterion, and of the order of 60 percent when based on the latter.

Based on the two criteria, Figures 19 and 20 show how the electrical energy supplied to the accelerator during the time ( $t_m$ ) is proportioned among (A) increasing the kinetic energy of the test gas slug, (B) dissipation at the electrode surface due to the voltage drop associated with the electronic processes taking place within the boundary layer, (C) ohmic heating of the gas, and finally (D) the remainder of the input power, which is assumed to represent boundary layer losses. Part of this last loss (E) is due to current densities larger than the free stream value passing through the Hartmann boundary layer and another part (F in Figure 19) represents the energy associated with the current passing through the gas in Region 2A. This fraction (F) will not show up in

Figure 20 since for the criterion used in that Figure the current  $J_{2A}$  is not assumed to compensate for boundary layer losses in the test slug. As was assumed in analyzing the measured open circuit voltage, it is assumed that the Hartmann layer is of constant thickness  $\delta_H = \sqrt{\mu/(\sigma B^2)}$  along the length of the electrodes and that the conductivity of the gas in these boundary layers is the same as the free stream gases. Furthermore, if it is assumed that the induced electric field in this region varies linearly from zero at the wall to the free stream value at a distance  $\delta_H$  then the percent of input power that is effectively dissipated in the Hartmann layer is given by the expression:

$$\frac{\int E(j - j_\infty) dy}{J \cdot \phi}$$

The relative size of the energy loss associated with the voltage drop at the electrode surface depends on the magnitude of the induced electrical field in the accelerator. This loss is as high as 45 percent of the input power for low values of the applied magnetic field and current (thus low values of  $uB_0h$ ) and as low as 5 percent for high values of applied field and current.

The percent of input power dissipated by ohmic heating of the gas depends on the ratio of "heating power" to "pushing power" ( $f = j/(\sigma uB)$ ) and thus for a given value of  $B$  this loss increases with increasing current, and for a given value of current this loss decreases with increasing

$B_0$ . This loss ranges from 2 percent to 13 percent of the input electrical power.

The total boundary layer loss is assumed to be the difference between the electrical energy supplied and the sum of A, B and C (Figures 19 and 20) in both criteria. Thus the percent of input energy lost due to boundary layers is in the range 55 to 40 percent depending on the power level if all the current is changed to accelerating the test slug and 25 to 10 percent if based only on the current flowing through the test gas. The estimated energy loss due to high current densities in the Hartmann boundary layer accounts for about 15 to 5 percent of the input electrical energy.

From Figures 19 and 20 it is to be noted that all but a few percent of the input energy is accounted for by summing the increase in kinetic energy of the slug, the energy loss associated with the electrode voltage drop, energy dissipated by ohmic heating of the test gas, energy associated with the fraction of current that passes through the cooler gas in Region 2A and the energy loss associated with high current densities in the Hartmann boundary layer. The portion of the input energy which is not accounted for is shown by crosshatching in Figures 19 and 20.

#### 8. Electrical Conductivity Measurements

Figure 21 shows the values of the electrical conductivity measured at stations 23" and 36" from the downstream end of the electrodes, respectively, as a function

of the square of the applied current for the full range of applied magnetic fields and an initial tube density of 2 mm. Hg. using argon as the working fluid. The curves labelled "equilibrium  $\sigma$ " in Figure 21 correspond to the conductivity for an equilibrium shock at the same initial tube density, and moving with constant velocity, the magnitude of this velocity being equal to the average observed front velocity downstream of the accelerator for each particular value of current and applied magnetic field. The experimental relation that was found to exist between the applied current magnetic field and downstream velocity was previously shown in Figures 11 and 12.

In order to calculate the equilibrium conductivity, the gas temperature was calculated from the conservation equations using the same procedure as in Reference 13. From the calculated temperature, the equilibrium conductivity is determined from Spitzer theory for a fully ionized gas<sup>(14)</sup>. Lin<sup>(9)</sup> has shown good agreement to result between this method of predicting the equilibrium conductivity and experimental results in shock heated argon over a range in conductivity up to about 60 mhos/cm. The upper limit of measured conductivities in the accelerator experiments was about 110 mhos/cm.

The curves labelled "heating" correspond to the conductivity that would result if the test slug was heated at constant volume, the heating rate being  $J^2 R$  and the time

of heating being equal to the time the slug spends in the electrode gas ( $t_m$ ). Since, for a given current the time ( $t_m$ ) decreases with increasing values of the applied magnetic field, an average value was used in constructing the "heating" curves, and a double arrow is used to indicate the extremities of the averaging.

Despite the relatively large scatter in the data, Figure 21 indicates that the measured values of the conductivity of the slug agree more closely with the values that are predicted on the basis of ohmic heating rather than if the gas was shock heated up to the equilibrium temperature for a normal shock moving at the same front speed. It should be pointed out here that the length of "new" fluid accumulated behind the shock front as the front passed along the electrode gap was about 3 cms for the short accelerator and about 7 cms for the long accelerator, and in addition, about another 7 cms of "new" fluid is accumulated as the shock travels to the station at which the electrical conductivity was measured.

The measured conductivities shown in Figure 21 correspond to the average conductivity over about the first 15 cms of the test gas slug. From the conductivity responses as well as the smear photographs, the first few cms. of gas appear, in some cases, to be somewhat hotter than the remainder of the gas. Nevertheless, the substantial increase in the observed conductivities for the long accelerator as

compared to the values observed for the short accelerator raises the question as to the mechanism which brought about this increase. Order of magnitude arguments rule out eddy currents as the possible source of the required substantial heating, since, as can be seen in Figure 21 the "total eddy current would have to be greater than  $J_T$ . The existence of shock waves in the flow within the accelerator could provide substantial heating of the gas. Photographic evidence of the flow within the accelerator would be necessary to verify the assumption of shock waves.

#### 9. Generator Experiments

Three experiments were run with the electrodes shorted through an external load instead of being connected to a capacitor bank. These experiments were run in argon and an initial density of 2 mm. Hg. The average shock speed was 4900 m/sec at the entrance to the generator section and 4500 m/sec. at the exit. The measured electrical conductivity downstream was about 25 mhos/cm as compared to the usual value of about 40 mhos/cm for open circuit runs.

The open circuit measured voltage was 125 volts. In all three experiments where current was drawn, the measured voltage across the gap was about 60 volts, the current had an average value of 5100 amps over the 150  $\mu$ -sec interval of current flow. This was an average output of 0.3 megawatt and an average (over entire electrode surface) current density of about 150 amps per  $\text{cm}^2$ .

The gap resistance was calculated to be  $1.82 \times 10^{-3}$  ohms, based on the geometry correction due to Fishman<sup>(11)</sup> and on the mean value of the upstream and downstream conductivity and assuming that the slug is entirely within the electrode gap. Thus the JR voltage drop within the gas accounts for only 9.3 volts of the 65 volt drop observed across the gap. The remaining 56 volts must be associated with the electronic processes that take place within the boundary layer at this current level.

It is interesting to note that current continues to flow through the external circuit for a time interval that approximately corresponds to the time required for the "ideal" slug length of argon to pass through the electrode gap. Since the driver gas behind the ideal argon-driver interface is about 75 percent helium, it will not be electrically conducting at the temperature available and thus no current will be able to flow across the gap when the driven gas is present.



#### IV. CONCLUSIONS

1. The experiments indicated that the eddy currents flowing in the gas as the gas leaves the magnetic field region do not appreciably decelerate the flow even when the magnetic Reynolds number is greater than unity. For these experiments, the total gas dynamic pressure was larger than the magnetic pressure.

2. The measured open circuit voltages were a few percent lower than the calculated values for a circular channel which indicates that there are no detrimental internal short circuit paths.

3. By apportioning the total current between the test gas and the cooler gas that follows, the momentum and energy can be balanced. This balancing indicates that the momentum of the "new" fluid accumulated behind the shock as it travels through the electrode gap is supplied by the gases behind the test slug so that the MHD body force associated with the current passing through the test gas appears to act on a slug of constant mass. Using this model of a test slug of constant mass all but a few percent of the electrical input energy supplied to the test gas can be accounted for by summing the increase in kinetic energy, the energy loss due to the electrode surface voltage drop, energy dissipated by ohmic heating and the energy loss associated with high current densities in the assumed Hartmann boundary layer.

4. The ratio of the measured to the ideal calculated increase in gas velocity may be taken as a measure of the "momentum efficiency" of the accelerator. If the current that passes through the test slug is charged to accelerating a slug of fixed mass then the momentum efficiency is about 90 percent for both the short and long accelerator.

5. The ratio of the increase in kinetic energy of the test gas to the input electrical energy may be taken as a measure of the energy conversion efficiency of the accelerator. If the electrical energy associated with the current flowing through the test gas is charged to accelerating a test slug of constant mass, then the energy conversion efficiency is about 70 percent for the long accelerator and about 50 percent for the short accelerator at power levels greater than 3 megawatts, and falls off at lower power levels.

6. The percent of electrical energy that must be charged as a loss due to the boundary layers in the machine decreases with increasing power level. The estimate of this loss indicates that it is about 25 percent at a power level of 1.0 megawatts and reduces to about 10 percent at a power level of 5 megawatts.

7. The measured increase in electrical conductivity of the accelerated gases is approximately accounted for by ohmic heating in the case of the short accelerator, whereas for the long accelerator the measured increase in conductivity is appreciably more than can be accounted for by ohmic heating

alone. This gives rise to speculation as to the possibility of standing shocks within the accelerator.

## APPENDIX A

Smear photographs of the flow downstream of the accelerator.

1. Ordinary shock tube flow, no applied current or magnetic field,  $p_1 = 2$  mm. Hg. short accelerator.

Figure 22A shows a horizontal smear photograph of the self luminosity of the test gas as it travels over the first 30" of glass channel downstream of the accelerator. The length of the luminous gas is seen to remain approximately constant despite the fact that at these operating conditions the slug should have ideally increased in length by an additional 10 cms.

Near the entrance to the glass channel the luminosity is lowest near the shock front but as the slug moves downstream this low luminosity region moves to the rear. One would expect this region of low luminosity to have a lower electrical conductivity than the remaining hot gas and this is seen to be the case from electrical conductivity measurements made near the downstream end of the glass channel (see Figure 9E) but this effect is not discernable in measurements made nearer the upstream end of the glass channel (see Figure 9A).

Figure 22B shows a vertical slit smear photograph of the flow at a station 11" downstream from the tail end of the electrodes. The luminosity does not vanish at the

same time over the entire channel cross section but rather begins to vanish at the top of the tube and ends at the bottom about 15  $\mu$  sec or 6 cms. later.

## 2. Acceleration Experiments

The smear photographs show that the gas in Region 2A which was seen to be non luminous for the ordinary shock tube flow has become luminous and has been accelerated to almost the same velocity as the gas immediately behind the shock front. Furthermore, in the vicinity of the "ideal" interface between the driver and driven gas the velocity decreases to its original upstream value. For the short accelerator the luminosity patterns indicate that the length of test gas (Region 2) is about the same downstream and upstream of the accelerator for low values of  $J_T$  whereas for high values of  $J_T$  no sharp luminosity boundary was observed which would indicate a slug length. For the long accelerator the downstream flow was observed to bear a closer resemblance to "slug flow" than in the case of the short accelerator, that is to say, the flow was characterized by a hot slug of gas followed by a much longer length of appreciably cooler gas.

For the short accelerator when no magnetic field was applied externally as well as for experiments with an externally applied magnetic field but low currents, a region of low luminosity was observed a few cms behind the shock front.

At sufficiently high accelerations the shock front was observed to undergo a rapid decrease in velocity downstream of the accelerator. In most cases this speed adjustment took place in one step about ten diameters downstream from the electrodes, although in a few cases two such speed adjustments were observed. Also at sufficiently high accelerations the shock front was considerably distorted.

The only appreciable difference between the photographs for the air and argon experiments was that the shock front velocity in air decreased rapidly in a continuous rather than step fashion as the shock moved over the first half of the glass channel.

A.  $B_0 = 0$ , short accelerator, working fluid argon,  
 $p_1 = 2$  mm Hg.

Figure 23A shows a vertical slit picture for  $J_T = 7,500$  amps and  $B_0 = 0$  taken at a station 11" from the end of the electrodes. The region of low luminosity is clearly visible and extends from 1 to 4 cms behind the shock front. The length of test slug is seen to be about 15 cms. The gases in Region 2A contain "patches" of gas with high local luminosity which show up as streaks on the horizontal slit pictures. Furthermore the slope of these streaks should represent, and thus provide a measure of, the average local gas velocity. A summary of gas velocities measured by means of these streaks is given in Table IV of the text.

Figure 23B shows a horizontal smear photographs for  $J_T = 20,700$  amps and  $B_0 = 0$ . The shock front has a constant speed of about 6,450 m/sec of 1.36 times the upstream value. The slope of the "luminosity front" at the rear of the region of low luminosity is constant and corresponds to a velocity of 5,700 m/sec. This luminosity front is obviously a gas front and not a shock front.

B.  $B_0 = 5, 10, 15$  kilogauss, short accelerator, working fluid argon  $p_1 = 2$  mm Hg.

Over the range of applied magnetic field and characteristics of the smear photographs did not vary appreciably for a given value of applied current. Therefore, only two representatives vertical and horizontal photographs are reproduced here one of each at a low and a high value of the current.

Figures 24A and B show vertical smear photographs taken 11" downstream from the electrodes for  $J_T = 4,500$  amps,  $B_0 = 10$  kg and  $J_T = 11,800$  amps,  $B_0 = 10$  kg. respectively. From the lower current experiment the shock front is seen to be normal to the tube walls and the luminosity begins to diminish near the walls while the core of the gas remains luminous for an additional 2 diameters. The photographs for the higher current run shows the shock front to be considerably distorted and that the luminosity diminishes

first in the core of the flow and finally at the tube walls some 20 diameters later.

Figures 25A and B show horizontal smear photographs for  $J_T = 6,300$  amps,  $B_0 = 10$  kg and  $J_T = 17,800$  amps,  $B_0 = 10$  kg respectively. Near the entrance to the glass channel the luminosity pattern indicates a slug length of about 17 cms for the lower current run whereas for the higher current run it was not possible to distinguish a slug length. A region of low luminosity a few cms. behind the shock is visible in the lower current photographs whereas no such regions appears in the case of high current runs.

C.  $B_0 = 10, 15$  kilogauss, long accelerator, working fluid argon,  $\rho_1 = 2$  mm Hg.

Figure 26 shows a horizontal smear photograph for  $J_T = 16,500$  amps and  $B_0 = 15$  kilogauss. A rapid change in shock front speed is clearly visible about 10 diameters downstream from the electrodes. The shock front speed is about 11,600 m/sec before the velocity adjustment and about 8,500 m/sec afterwards. The luminosity pattern of the photograph indicates a slug length of 14 cms.

D.  $B_0 = 10$  kilogauss, long accelerator, working fluid air,  $\rho_1 = 2$  mm Hg.

Figure 27 shows a horizontal smear photograph for an experiment in air where  $J_T = 18,000$  amps,  $B_0 = 10$  kg. The shock front velocity is seen to decrease in a smooth



rapid manner near the entrance to the glass channel. Over the first 7" of visible flow the shock front velocity decreased from about 16,000 m/sec to about 9,500 m/sec.

### 3. Multiple Shock Pattern

In about 10 percent of the experiments with the short accelerator two and sometimes three shocks were observed in the smear photographs and the electrical conductivity measurements. Figure 28 shows a horizontal smear photograph of an experiment using argon at  $p_1 = 2$  mm Hg. as the working fluid with  $J_T = 11,400$  amps and  $B_0 = 15$  kilogauss. The velocity of the first and second shock near the entrance to the glass channel are 8,420 m/sec and 10,700 m/sec respectively. Both shocks slow down as they move downstream but the second shock slows considerably more than the first with the result that at the downstream end the two shock speeds are 7000 and 7,900 m/sec respectively.

REFERENCES

1. Camac, M., Kantrowitz, A. Petschek, H. E., Plasma Propulsion Devices for Space Flight. Avco Research Laboratory Research Report No. 45, February 1959
2. Fay, J.A., Janes, G.S., Keck, J.C., Low Temperature Viscously Contained Accelerator, Avco Research Laboratory Report, Research on Plasma Propulsion, December 1959
3. Sutton, G.W. Electrical and Pressure Losses in Magneto-hydrodynamic Channels Due to End Current Loops, General Electric Co. Report R59SD431 (1959)
4. Demetriades, S.T., Experimental Magnetogasdynamics Engine for Argon, Nitrogen and Air., Presented at the Second Symposium on Engineering Aspects of MHD, Univ. of Penn (1961)
5. Carter, A.F., Wood G.P., Sabol, A.P., Weinstein, R.H., Experiments in Steady State High Density Plasma Acceleration Presented at the Second Symposium on Engineering Aspects of MHD, Univ. of Penn. (1961)
6. Ragusa, D., Baker, J., Experimental Results with a Direct Current Electromagnetic Plasma Accelerator. Presented at the Second Symposium on Engineering Aspects of MHD, Univ. of Penn. (1961)
7. Wood, G. P., Carter, A.F., Arlen, F., Considerations in the Design of a Steady DC Plasma Accelerator. Dynamics of Conducting Gases, ed. by Ali Bulent Cambel and John B. Fenn, North eastern Univ. Press (Evanston), 1960
8. Fay, J.A., Hogan, W.T., Heat Transfer to Cold Electrodes in Flowing Ionized Gas., Presented at the Second Symposium on Engineering Aspects of MHD, Univ. of Penn (1961)
9. Lin, S.C., Resler, E.C., Kantrowitz, A., Electrical Conductivity of Highly Ionized Argon Produced by Shock Waves., Jour. Applied Physics 26, 95 (1955)
10. Roshko, A., On Flow Duration in Low-Pressure Shock Tube. Phys. of Fluids Vol. 3 No. 6 Nov.-Dec. 1960
11. Fishmann, F. Steady Magnetohydrodynamic Flow Through a Channel of Circular Section., Avco Research Laboratory Report No. 97, December 1960

12. Moffatt, W.C., Boundary Layer Effects in Magnetohydrodynamic Flows, ScD. Thesis M.I.T., June 1961
13. Resler, E.L., Lin, S.C., Kantrowitz, A., The Production of High Temperature Gases in Shock Tubes, Jour. Applied Phys. 23, 12 (1952)
14. Spitzer, L., Harm, R., Transport Phenomena in a Completely Ionized Gas., Phys. Rev., 89, 977 (1953)
15. Amdur, I., Mason, E.A., Properties of Gases at Very High Temperatures, Phys. of Fluids, Vol. 1, No. 5, Sept-Oct. 1958

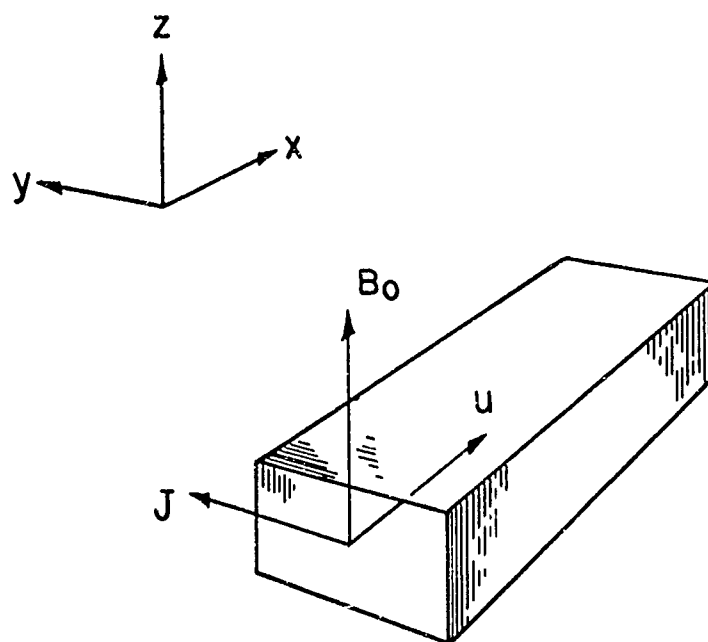


Fig. 1. Magnetogasdynamic channel

Fig. 2. a. Shock tube accelerator experiment, schematic  
b. Accelerator crosssection  
c. Accelerator

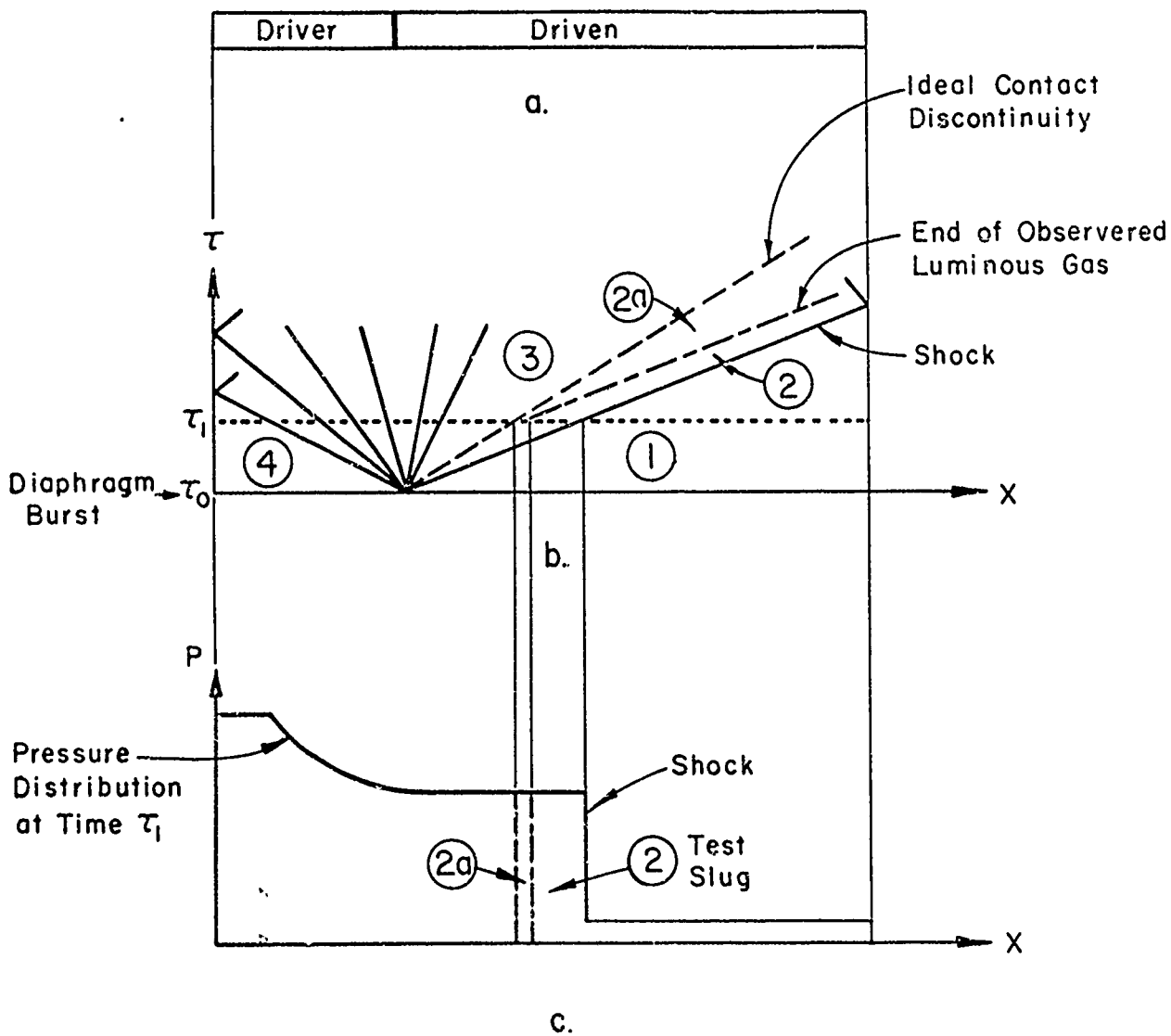


Fig. 3. a. Schematic of conventional shock tube  
b. x-t diagram showing shock front and expansion wave after diaphragm opens  
c. Pressure distribution along shock tube time  $t_1$ .

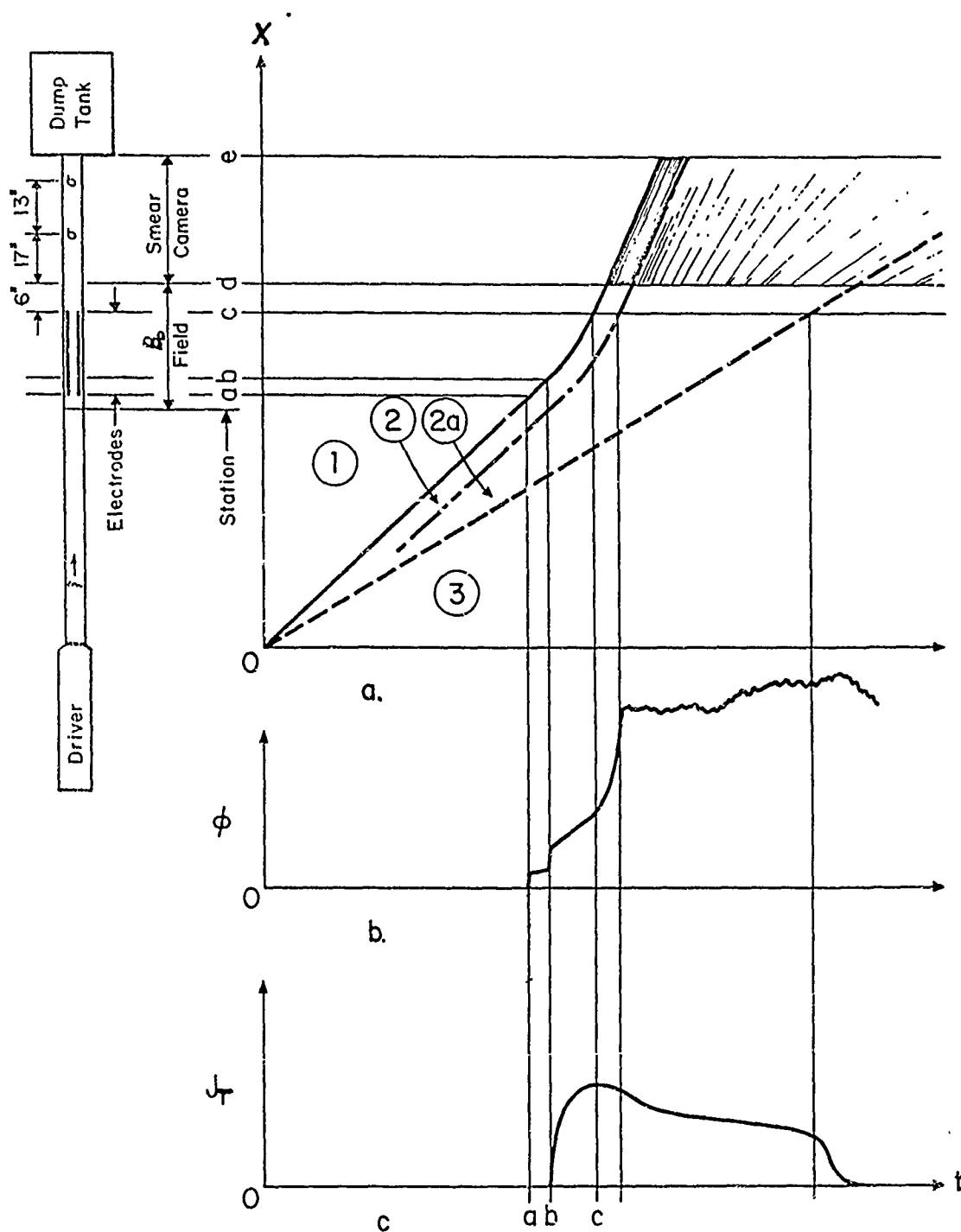


Fig. 4. a. x-t diagram of shock tube flow with accelerator in operation. The flow between stations d and e was photographed with a smear camera and a representative sketch of the luminosity pattern is shown on the x-t plane, the streaks result from spots of high local luminosity.  
b. Representative sketch of the voltage drop across the electrodes vs time.  
c. Representative sketch of the total current vs time.



$B_0 = 5$  kg.  
Vertical 100 volts/.6 cm.  
Sweep  $50 \mu$  sec. / cm.



$B_0 = 10$  kg.  
Vertical 50 volts/cm.  
Sweep  $50 \mu$  sec./cm.



$B_0 = 15$  kg.  
Vertical 100 volts/cm.  
Sweep  $50 \mu$  sec/cm.

Fig. 5 Open circuit vs. time responses for the short accelerator using argon at  $p = 2$  mm Hg. and magnetic fields of 5, 10, and 15 kilogauss.



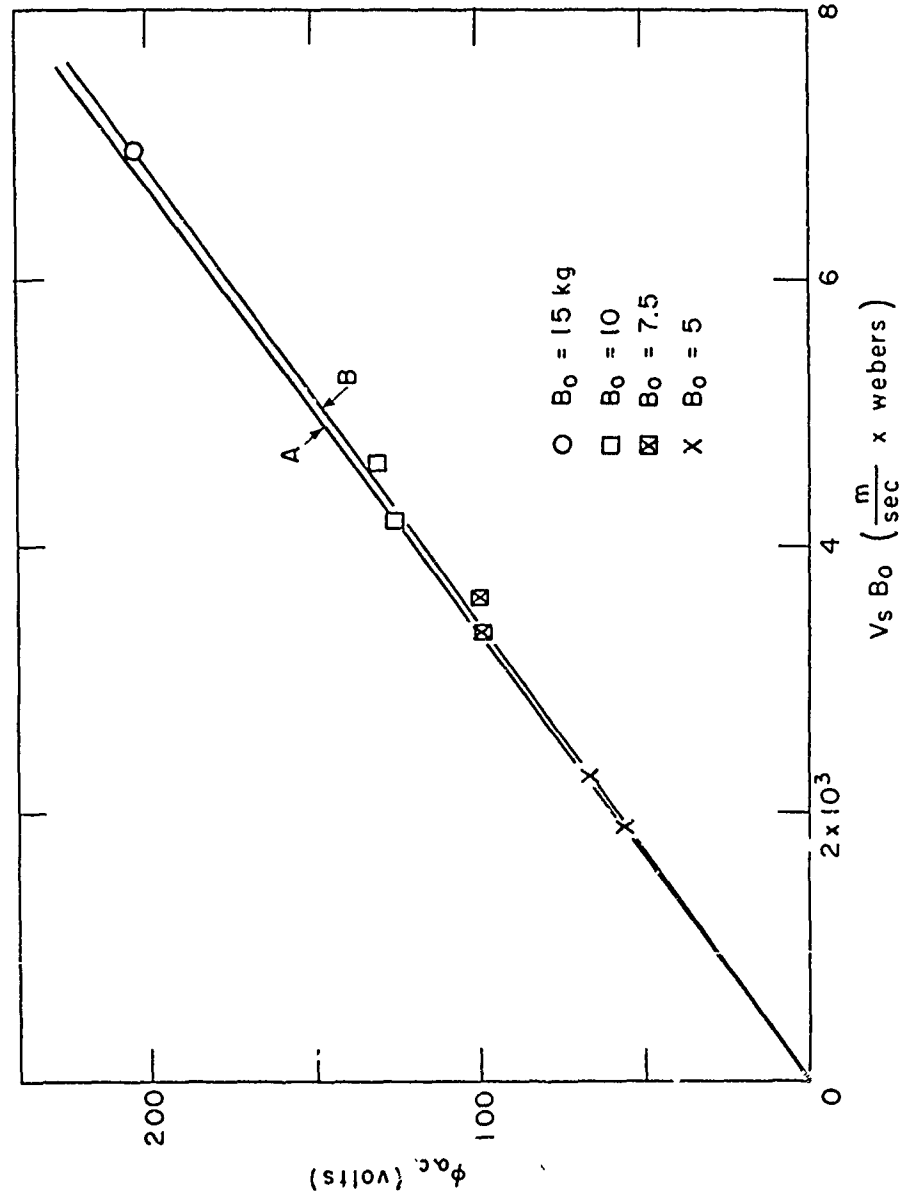


FIG. 6. Measured open circuit voltage vs the product of shock velocity and applied magnetic field for argon at  $p=2\text{mm Hg}$ . Curve A represents the ideal back emf ( $\frac{V_s B_0}{\mu_0}$ ) based on the calculated effective electrode separation ( $h$ ). Curve B represents the correction for short circuit currents flowing through an assumed Hartmann boundary layer of constant thickness ( $\delta_H$ ) and having a conductivity equal to the free stream value.

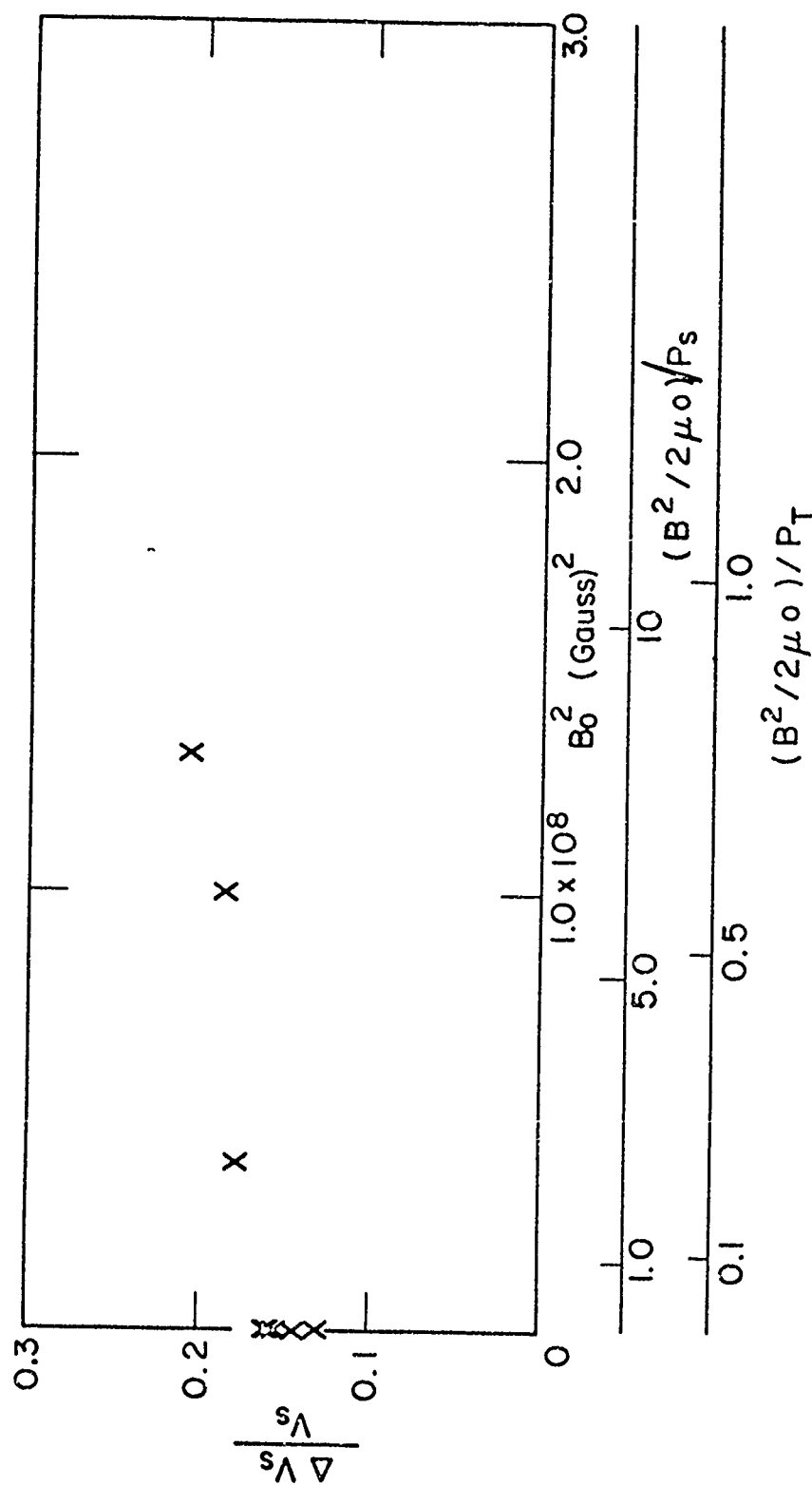


FIG. 7. Measured shock speed attenuation over 5.5 feet of channel including the short accelerator vs applied magnetic field. In these experiments the electrodes were removed, the incident shock was Mach 15,  $\rho = 1 \text{ mm Hg}$  and argon was the working fluid.

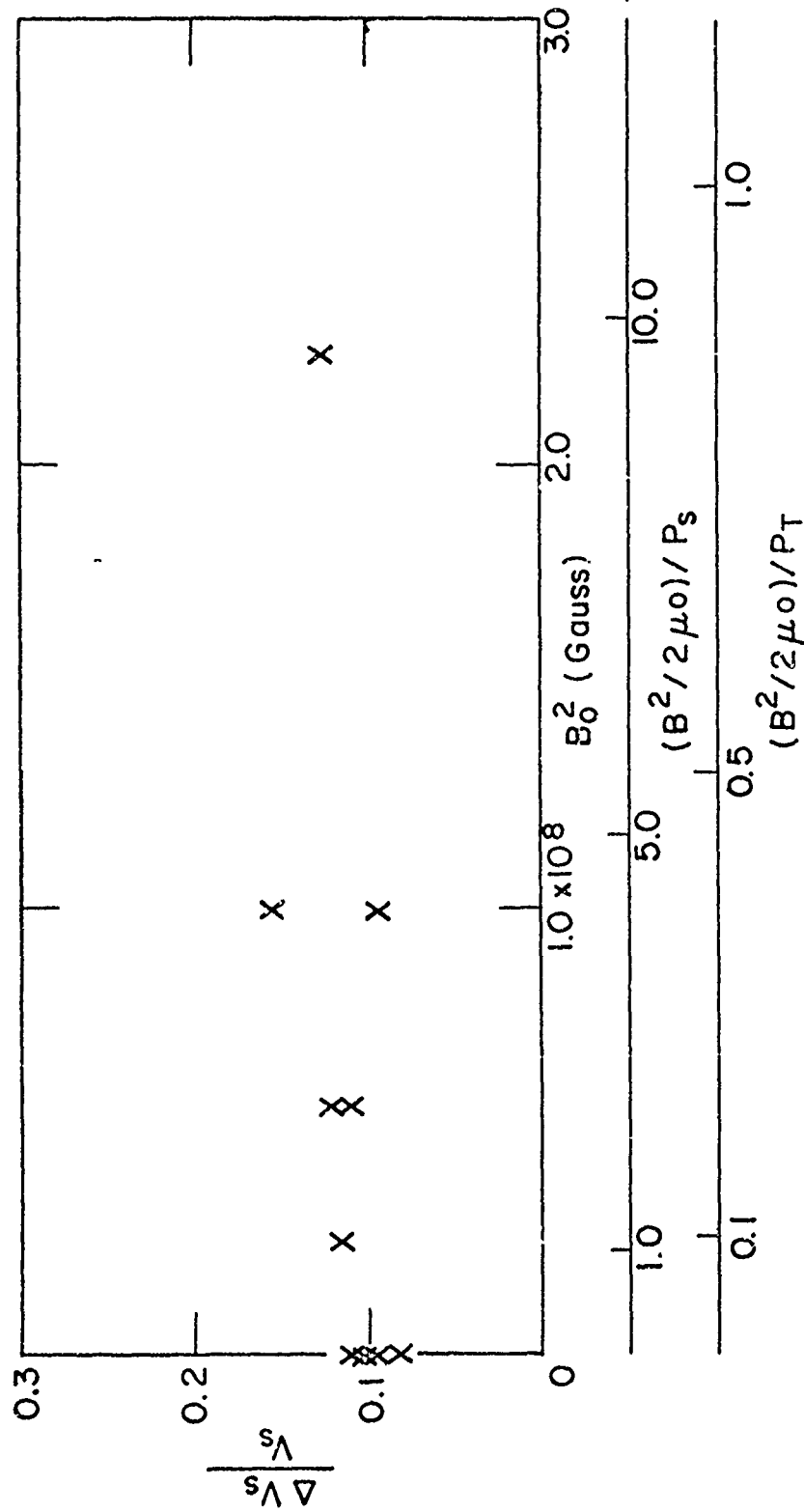
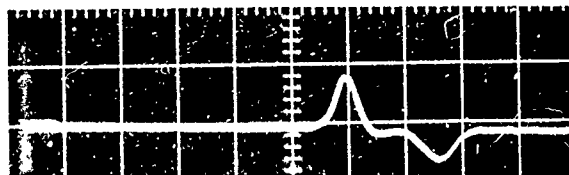
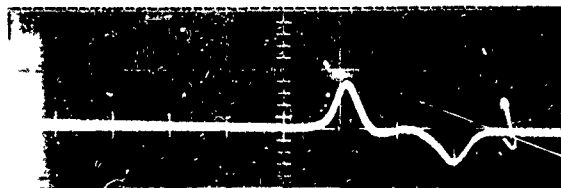


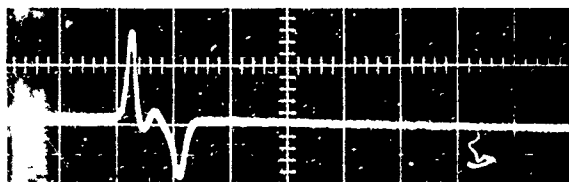
Fig. 8. Measured shock speed attenuation over 5.5 feet of channel including the short accelerator vs applied magnetic field. In these experiments the electrodes were in place, the incident shock was Mach 15,  $\mathcal{J} = 2\text{mm Hg}$  and argon was used as the working fluid.



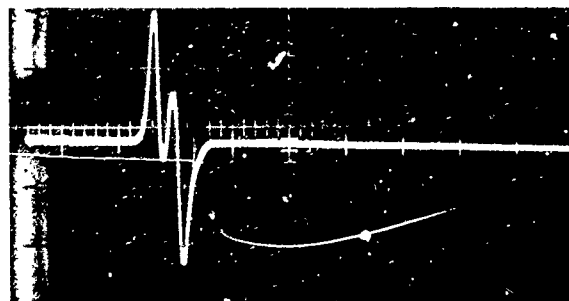
Bo 0  
Vert. 2 v/cm  
Sweep 20  $\mu$ s/cm



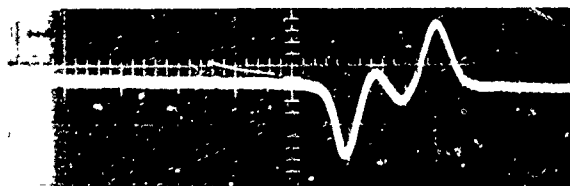
Bo 5 kg  
Vert. 2 v/cm  
Sweep 20  $\mu$ s/cm



Bo 7.5 kg  
Vert. 1 v/cm  
Sweep 50  $\mu$ s/cm



Bo 10 kg  
Vert. .5 v/cm  
Sweep 50  $\mu$ s/cm



Bo 0  
Vert. 1 v/cm  
Sweep 20  $\mu$ s/cm

Fig. 9

Electrical conductivity gage responses at various values of  $B_0$  using argon at  $\approx 2$  mm Hg. The gage was located 23" downstream from the electrodes for (a) through (b) and 36" downstream for (c).

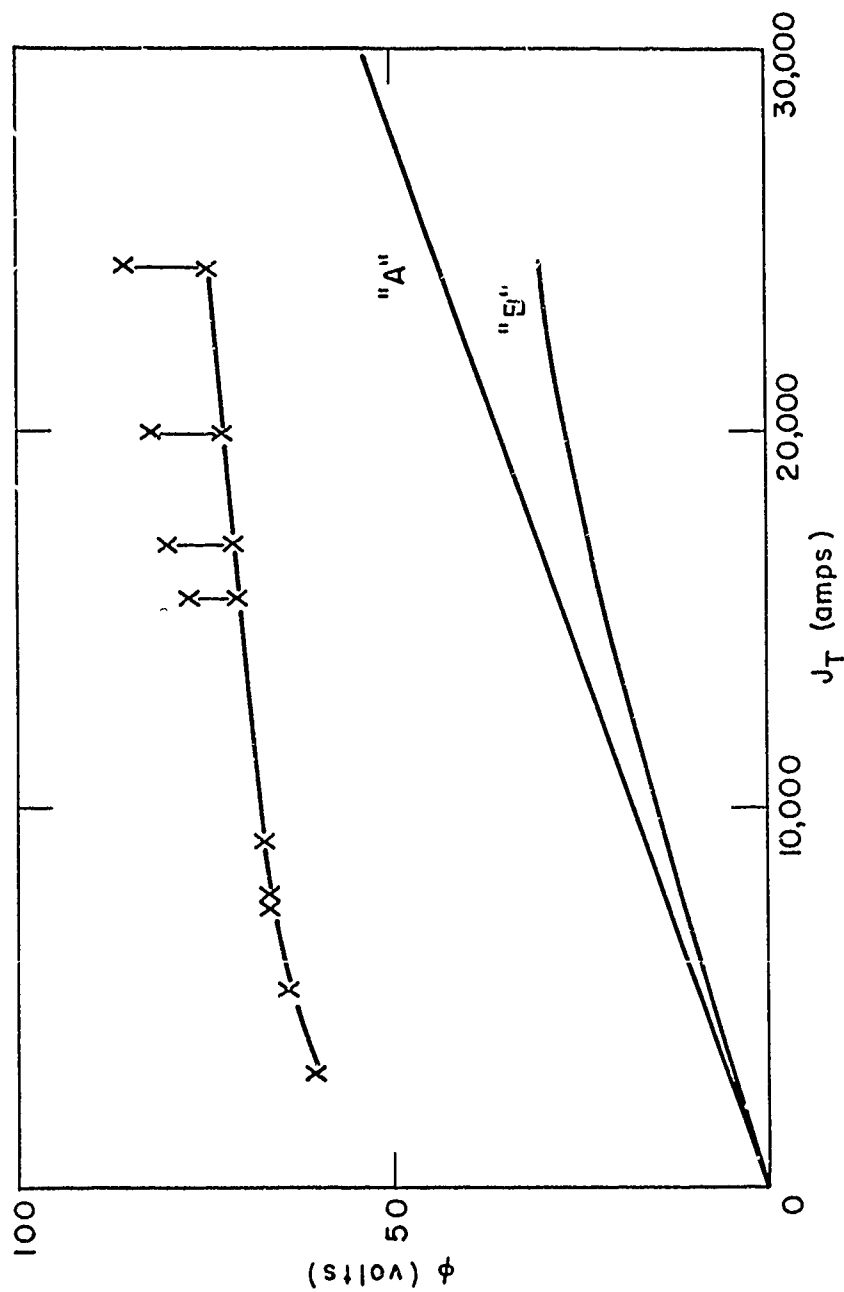


Fig. 10. Measured voltage drop across electrodes vs total current for the short accelerator using argon at  $J_0 = 2 \text{ mm Hg}$  and  $B_0 = 0$ . The vertical bars represent the increase in voltage due to the back emf associated with the backstrapping effect. Curve A is the gas resistance assuming the conductivity remains at its upstream value whereas Curve B assumes the conductivity to be equal to the mean of the upstream and downstream value.

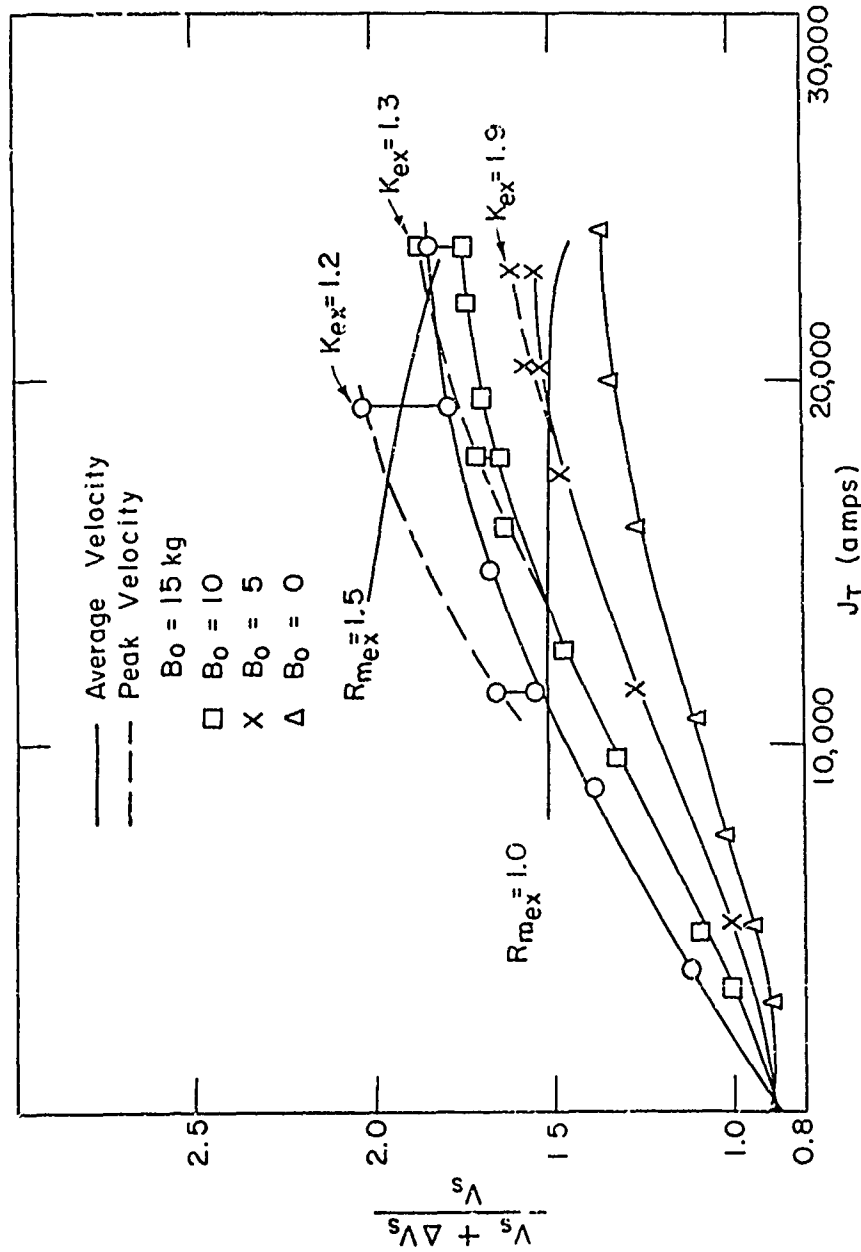


FIG. 11. Measured increase in shock front velocity vs total current for the short accelerator using argon at  $p = 2 \text{ mm Hg}$ . Peak and average velocities apply to approximately the first 8 and 24 diameters downstream of the accelerator respectively. The value of the channel loading parameter ( $K = \rho/4\delta\theta_0$ ) evaluated at the accelerator exit is shown for the maximum acceleration run. The value of the magnetic Reynolds number ( $R_m = 4\sigma r\theta_0$ ) evaluated at the accelerator exit is indicated by solid curves over the range of the experiments.

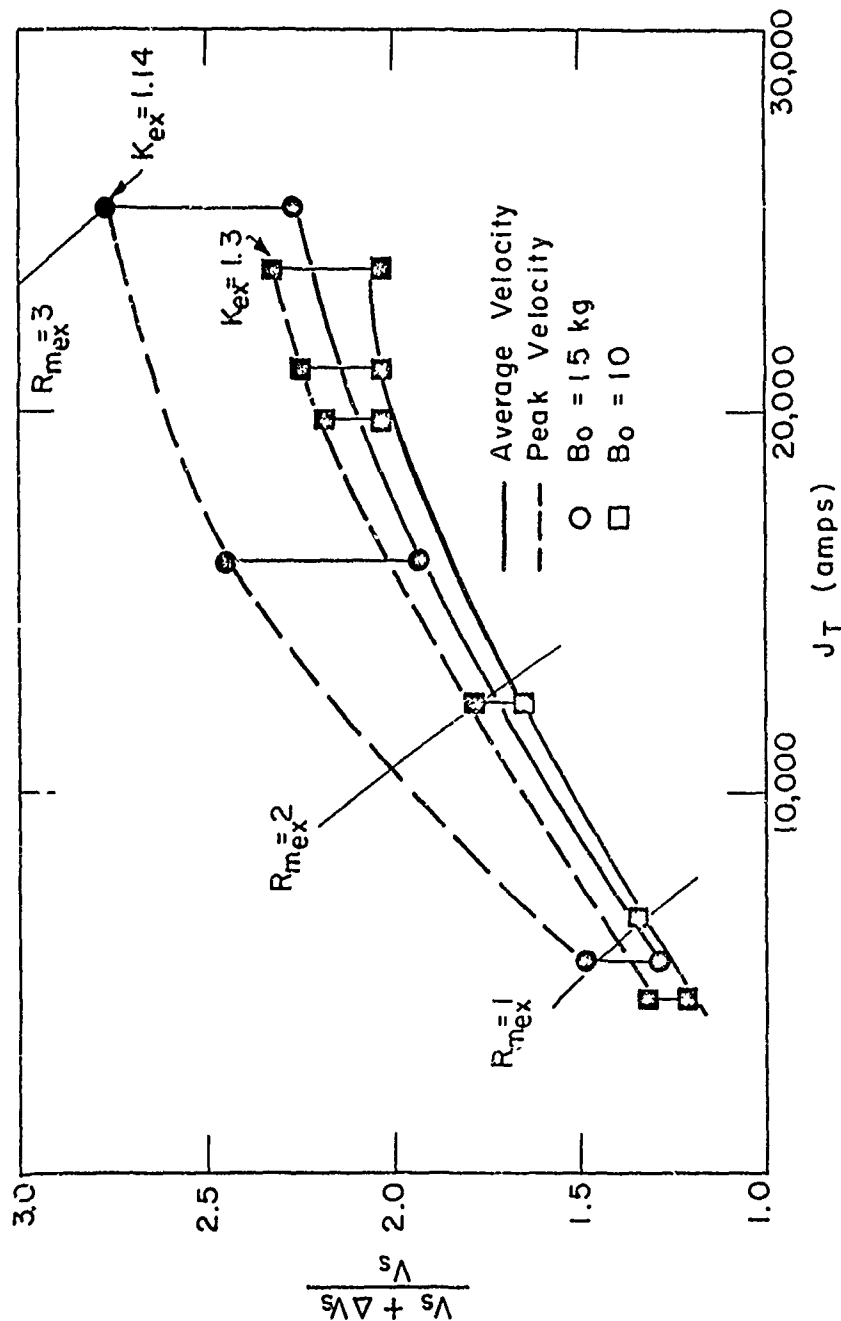


FIG. 12. Measured increase in shock front velocity vs total current for the long accelerator using argon at  $p = 2$  mm Hg. Peak and average velocities apply to approximately the first 8 and 16 diameters downstream respectively. The value of the channel loading parameter ( $K = \phi / \mu q h$ ) evaluated at the accelerator exit is shown for the maximum acceleration run. The value of the magnetic Reynolds number ( $R_m = \mu q r B_0$ ) evaluated at the accelerator exit is indicated by solid curves over the range of the experiments.

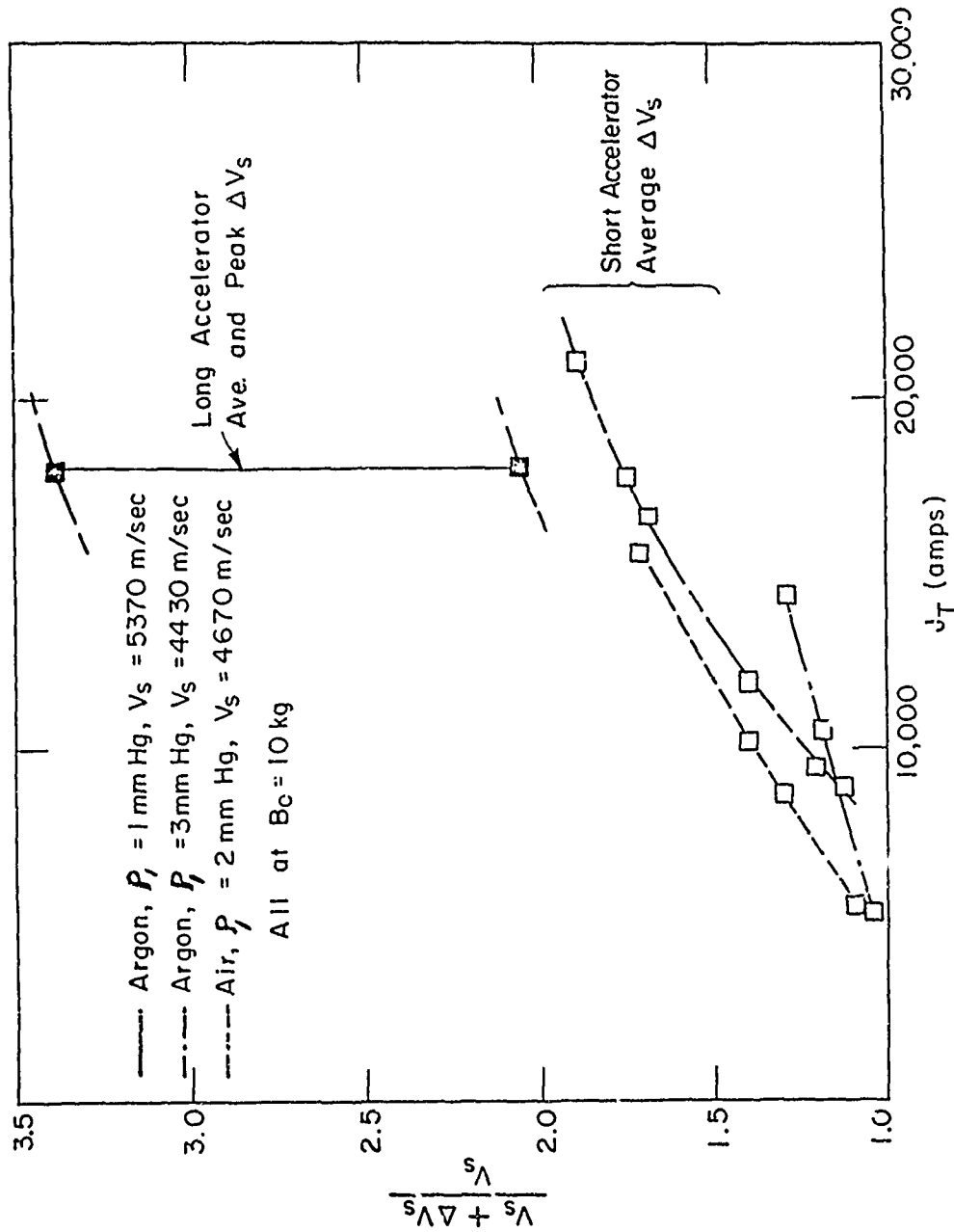


Fig. 13. Measured increase in shock front velocity vs total current for short and long accelerator using air and argon as the working fluid at various initial tube densities.



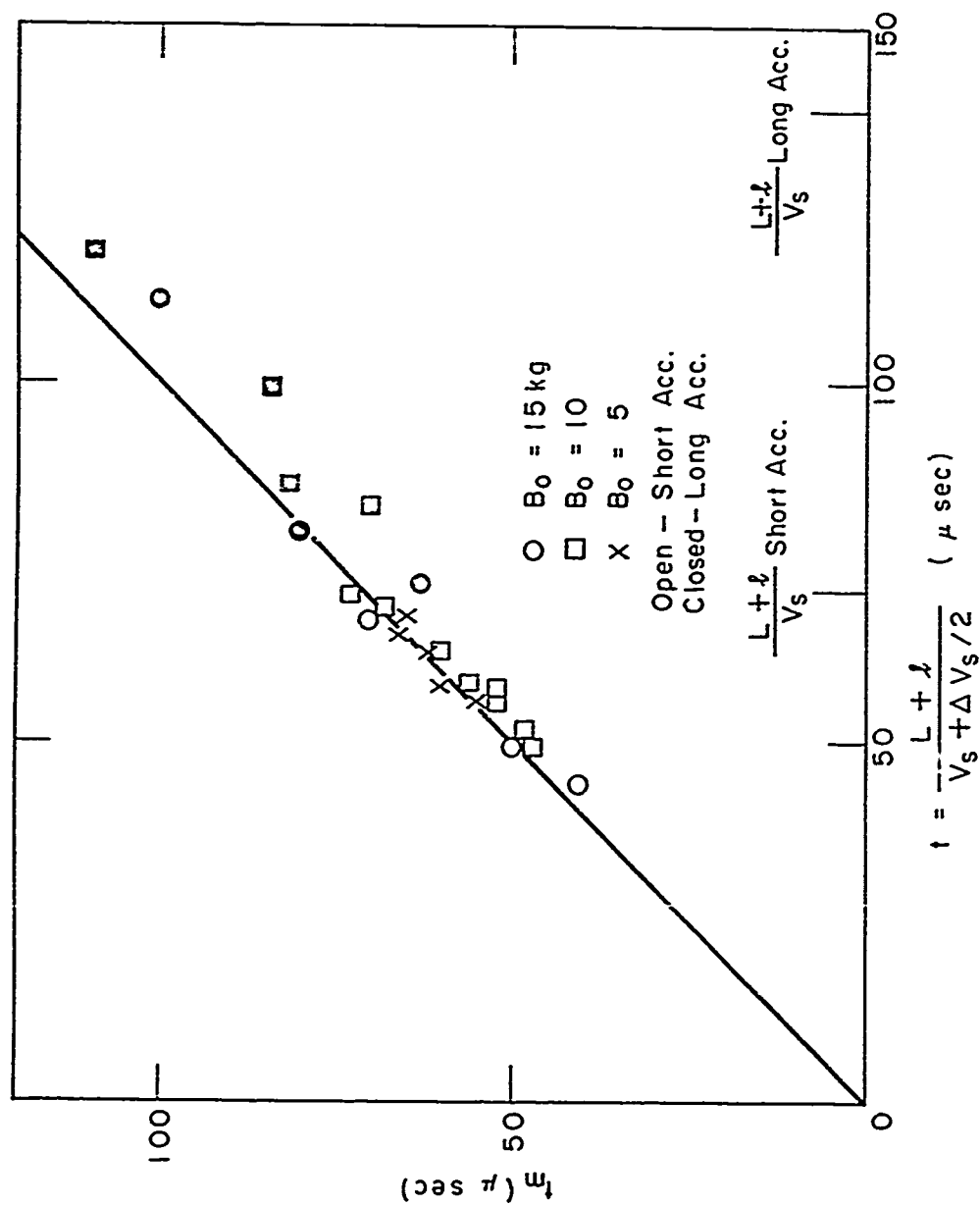


Fig. 14. Measured vs predicted time based on the slug model for the test gas to traverse electrode gap. Argon is the working fluid at  $\rho = 2 \text{ gm/cc}$ .

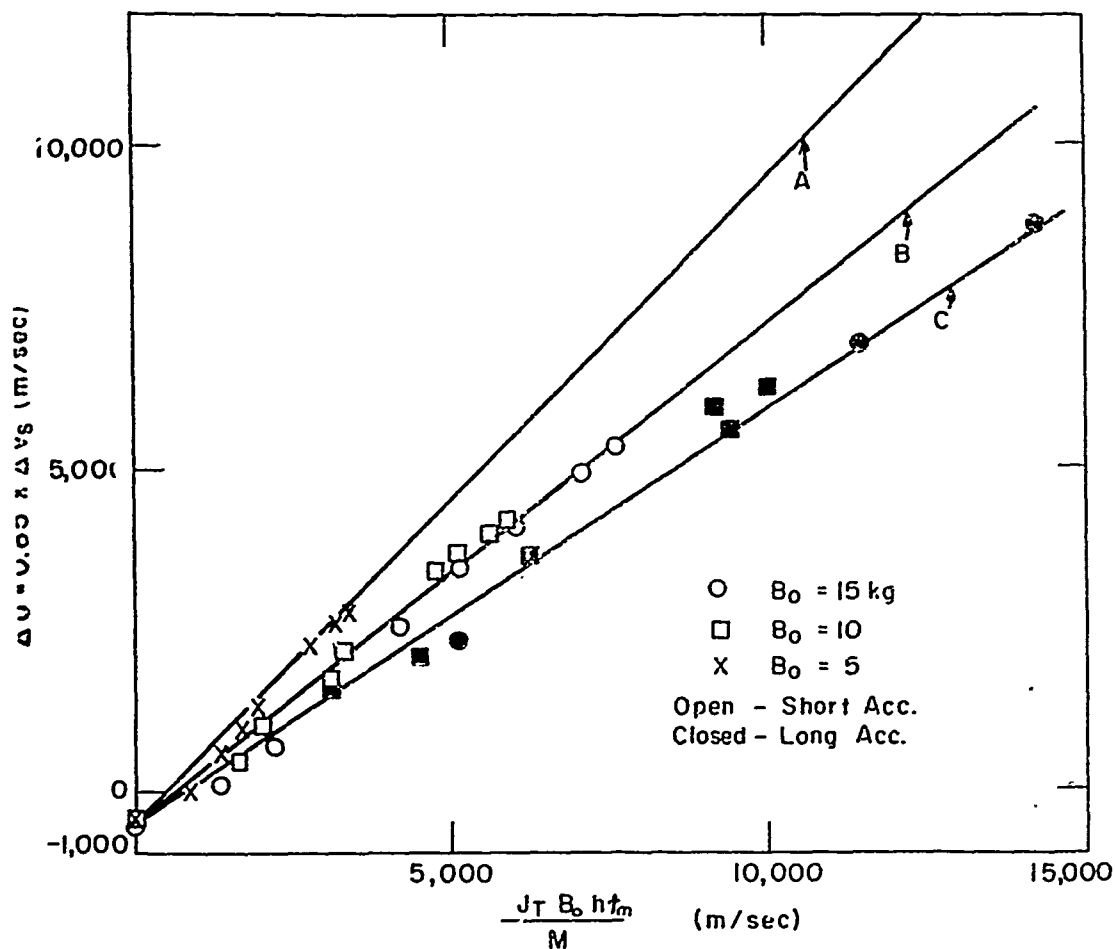


Fig. 15. Measured increase in velocity vs value predicted on the basis of the slug model of constant mass of argon,  $P = 2 \text{ mm Hg}$ . Curve A assumes that all the applied current passes through the test gas whereas Curves B and C, for the short and long accelerator respectively, assumes that some of the applied current passes through the gas in Re. ion 2A.

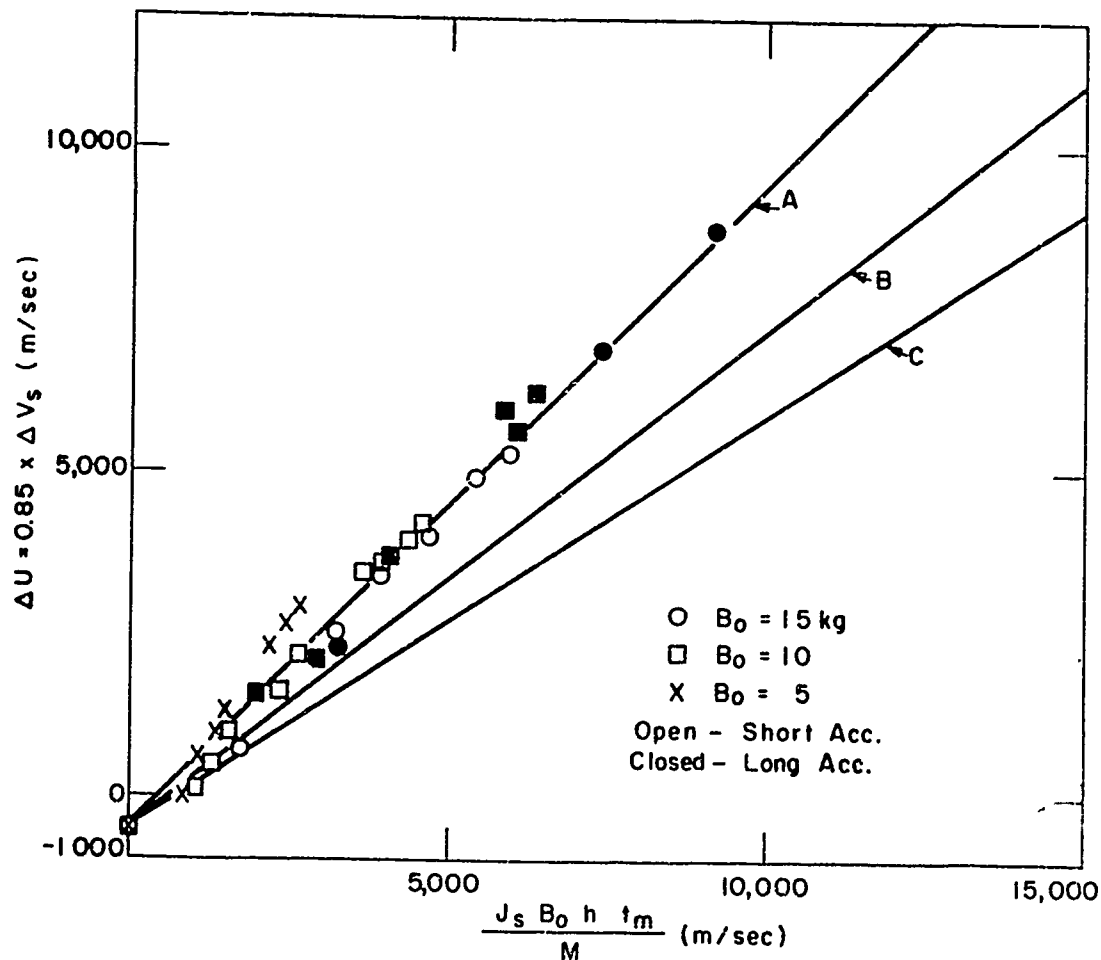


Fig. 16. Measured increase in velocity vs value predicted on the basis of the slug model for argon at  $P = 2 \text{ mm Hg}$ . Curve A is based on a slug mass equal to the upstream value  $M$ . Curves B and C are based on a slug of mass  $M$  plus the 'new' mass accumulated by the shock in the electrode gap of the short and long accelerator respectively.

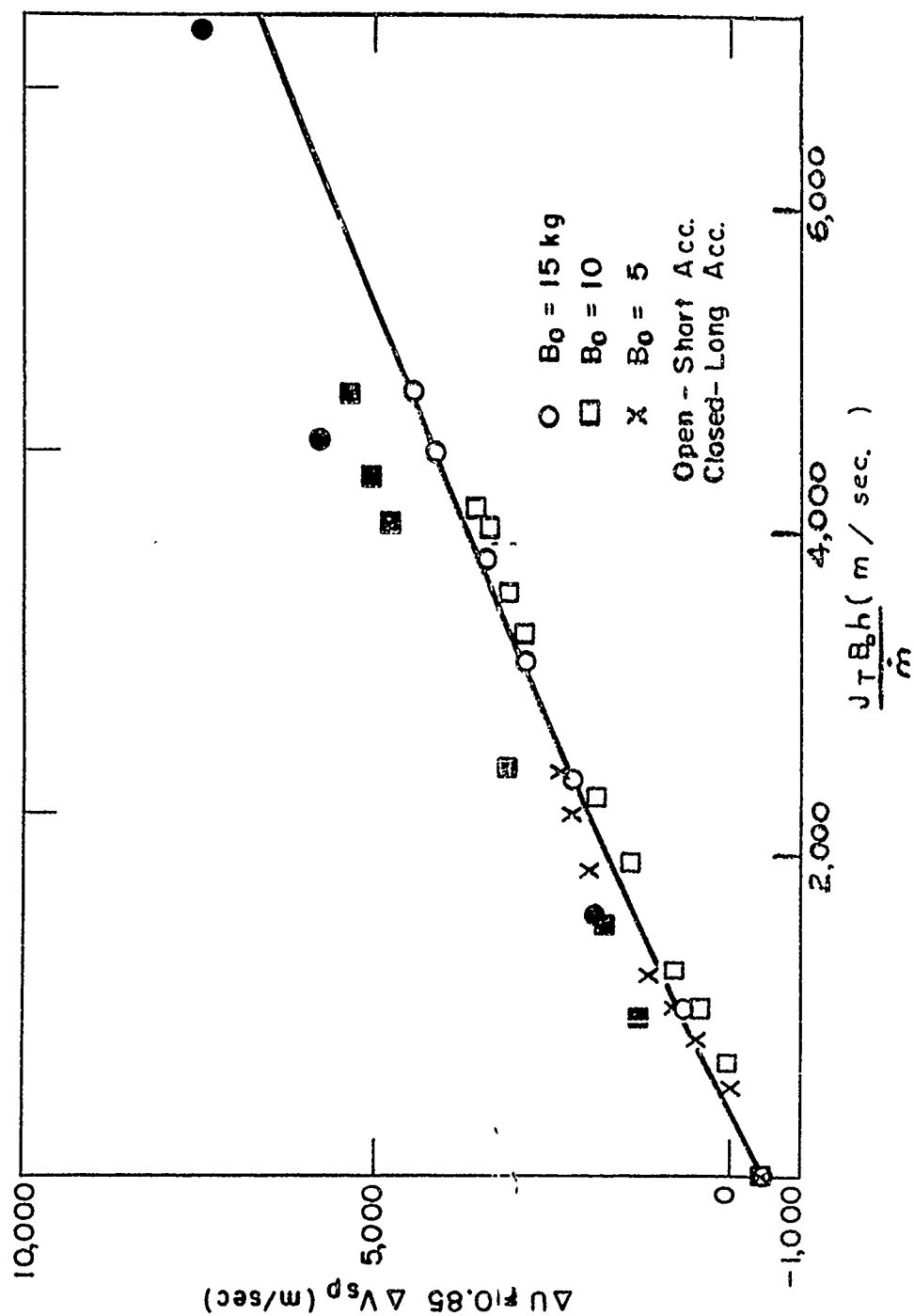


Fig. 17. Measured increase in velocity vs the parameter  $\frac{JTBh}{\dot{m}}$  for argon at  $p = 2 \text{ mm Hg}$ . The solid curve represents the ideal increase in velocity for steady state operation.

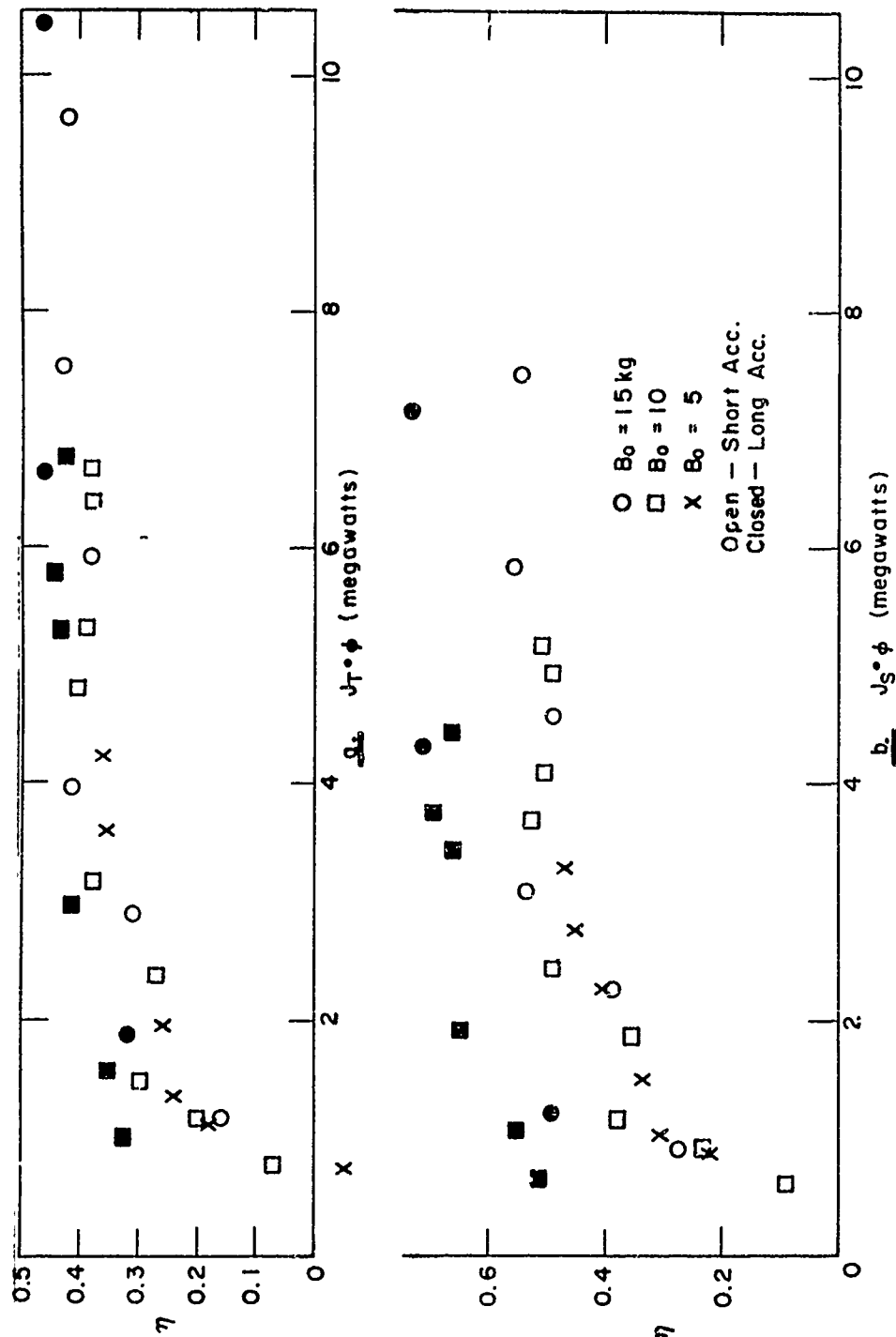


Fig. 18. Energy conversion efficiency vs electrical power supplied to the electrodes for argon at  $p = 2\text{mm Hg}$ . Fig. 18 a assumes that the total applied current must be charged to accelerating the test gas whereas in Fig. 18 b only the current that passes through the test gas is charged to accelerating the slug.

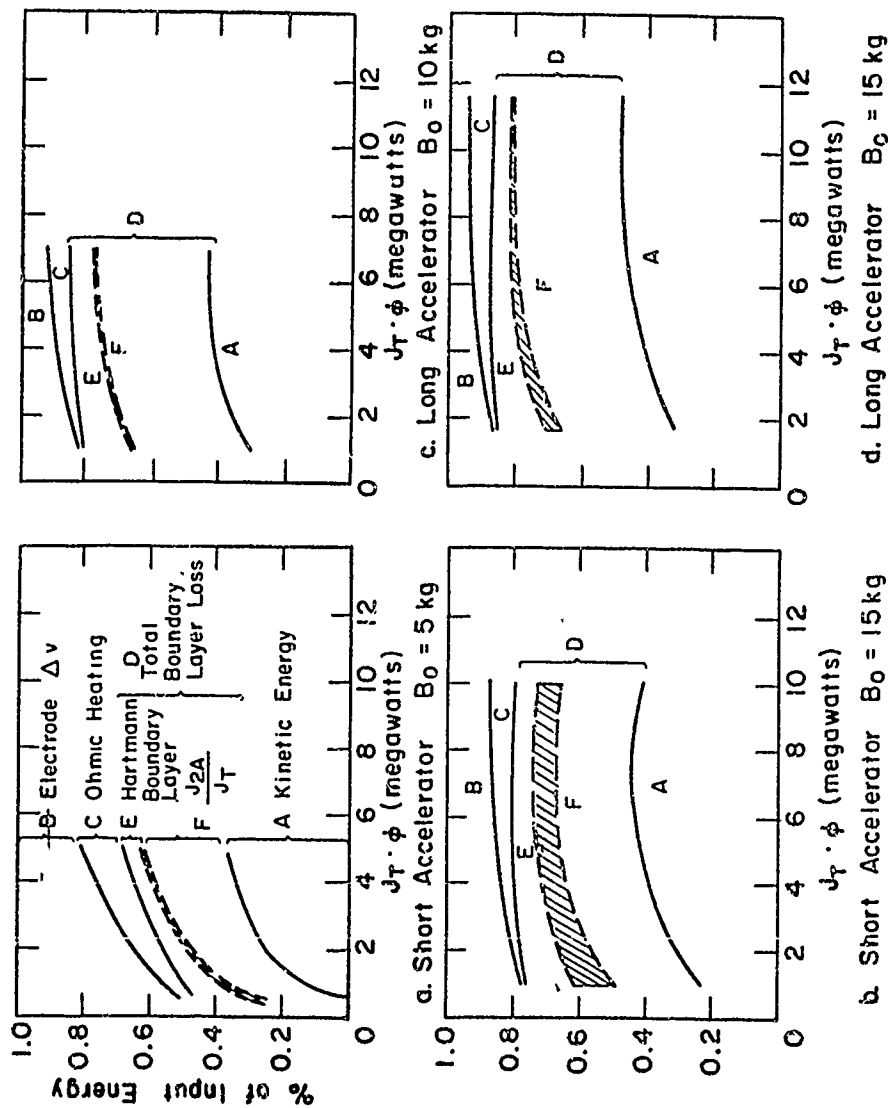


Fig. 19. Energy balance for argon at  $\rho_f = 2 \text{ mm Hg}$  based on the total current ( $J_T$ ) supplied to the electrodes. The crosshatched portion is the percent of energy unaccounted for after summing (A) the increase in kinetic energy of the slug (B) energy dissipated due to electrode voltage drop (C) energy dissipated in ohmic heating of the gas (E) energy dissipated as a result of short circuit currents in the Hartmann boundary layer and (F) energy associated with the current flowing through Region 2A. The total boundary layer loss (D) is assumed to be the difference between unity and the sum of (A), (B) and (C).

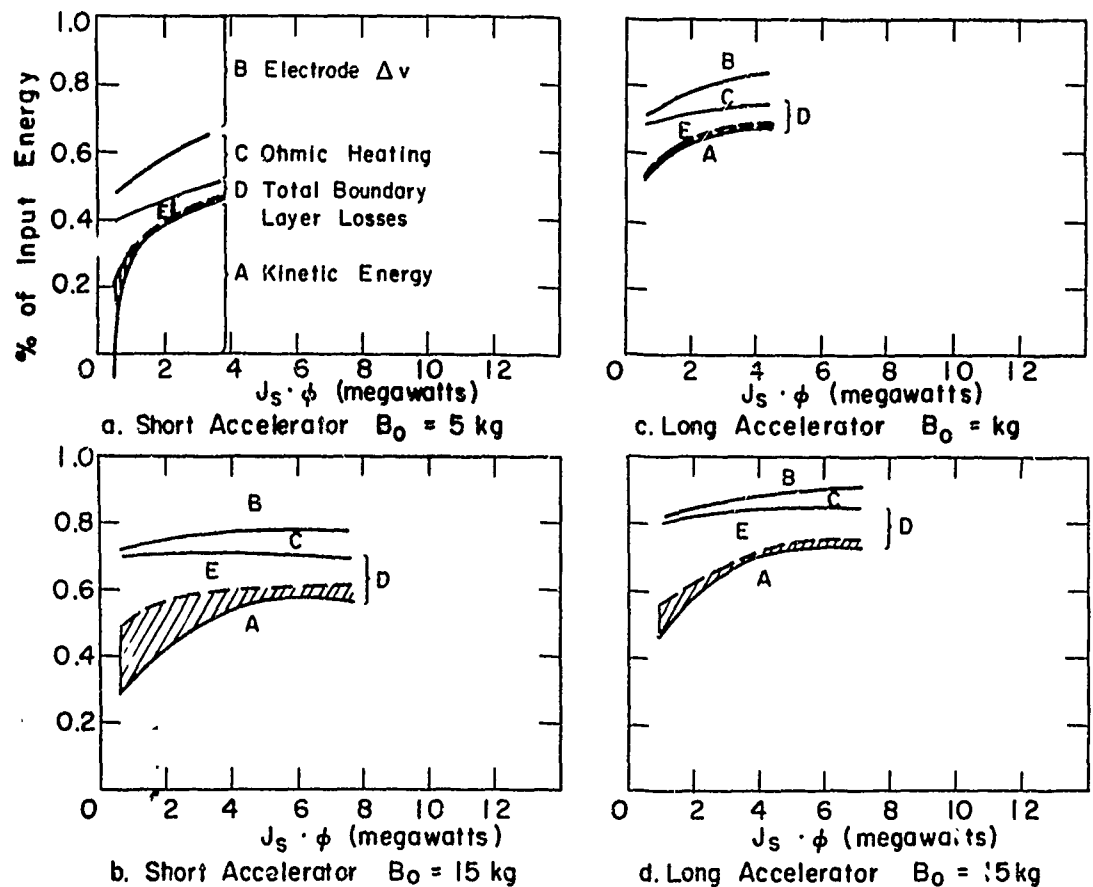


Fig. 20. Energy balance for argon at  $p = 2 \text{ mm Hg}$  based on the current ( $J$ ) passing through the test slug. The crosshatched portion is the percent energy unaccounted for after summing (A) the increase in kinetic energy of the slug (B) energy dissipated due to electrode surface voltage drop (C) energy dissipated in ohmic heating and (E) energy dissipated as a result of short circuit currents in the Hartmann boundary layer. The total boundary layer loss (D) is assumed to be the difference between unity and the sum of (A), (B) and (C).

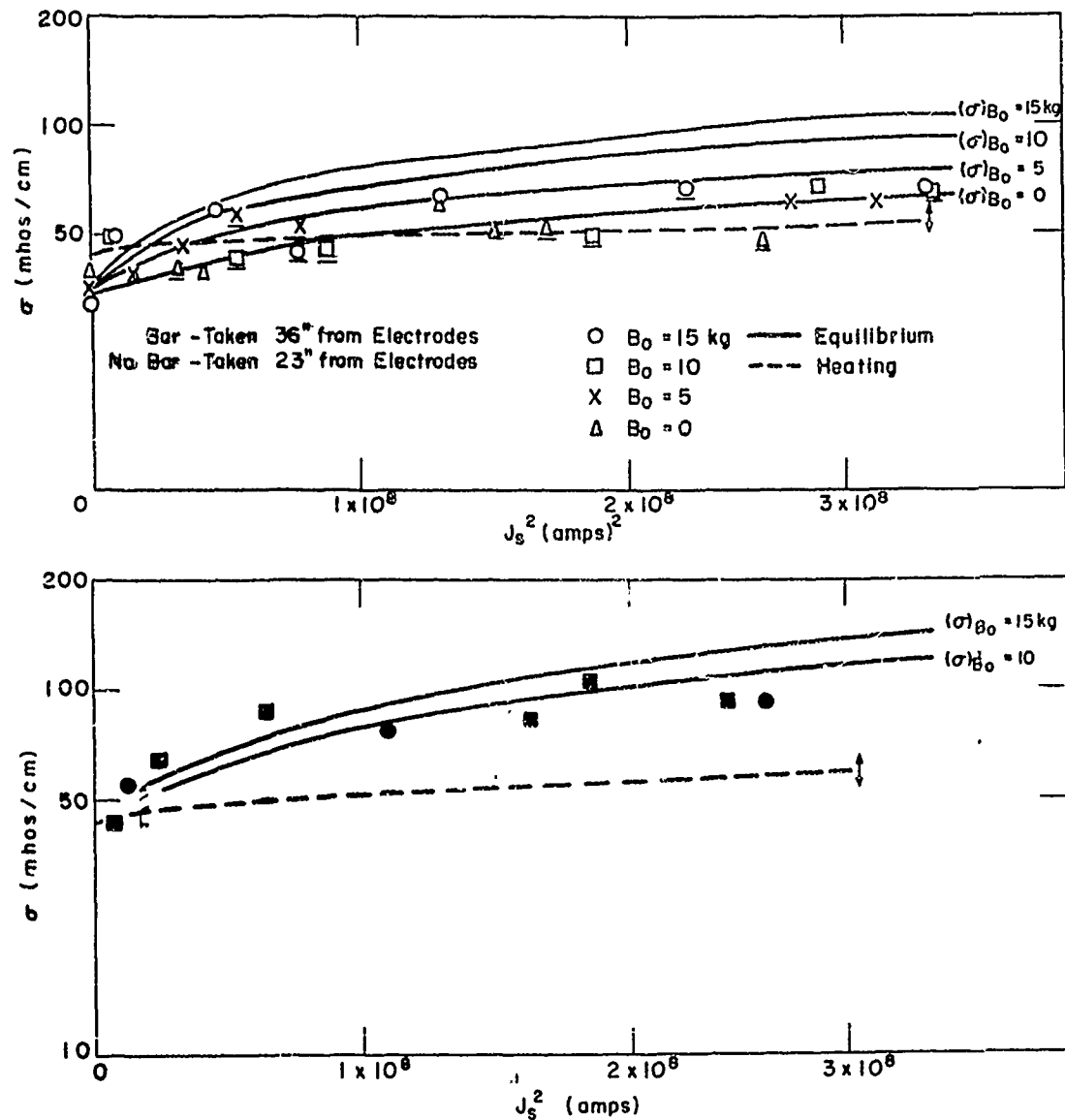
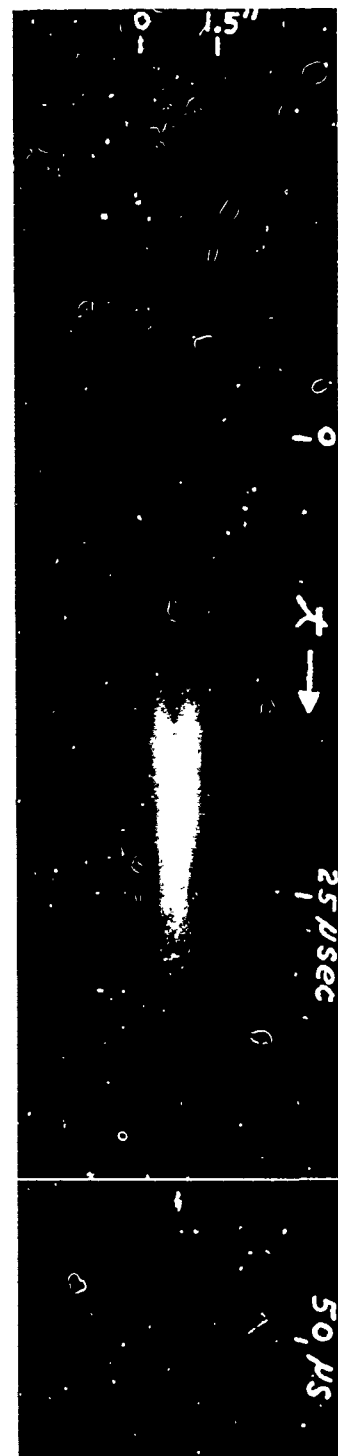


Fig. 21. Measured electrical conductivity downstream of the accelerator vs the square of the current flowing through the test gas. These experiments were run in argon at  $P = 2$  mm Hg. Fig. 21 a is for the short accelerator and 21 b for the long accelerator. The solid curves represent the conductivity for an equilibrium shock moving at the same speed. The dashed curves represent the conductivity that would result from ohmic heating of the gas at constant volume.





a.



b.

Fig. 22 Smear photographs of ordinary shock tube flow downstream of the short accelerator using argon at an initial density of  $P = 2$  mm Hg. Fig. 22 a. was taken through a horizontal slit starting at station d. Fig. 22 b. was taken through a vertical slit about 4 diameters from station d.



Fig. 23 Smear photographs of the flow downstream of the short accelerator with no externally applied magnetic field. Argon at  $P = 2$  mm Hg. was the working fluid. Fig. 23 a was taken through a horizontal slit starting at station d, and  $J_T = 7,500$  amps. Fig. 23 b was taken through a vertical slit about 4 diameters from station d, and  $J_T = 20,700$  amps.

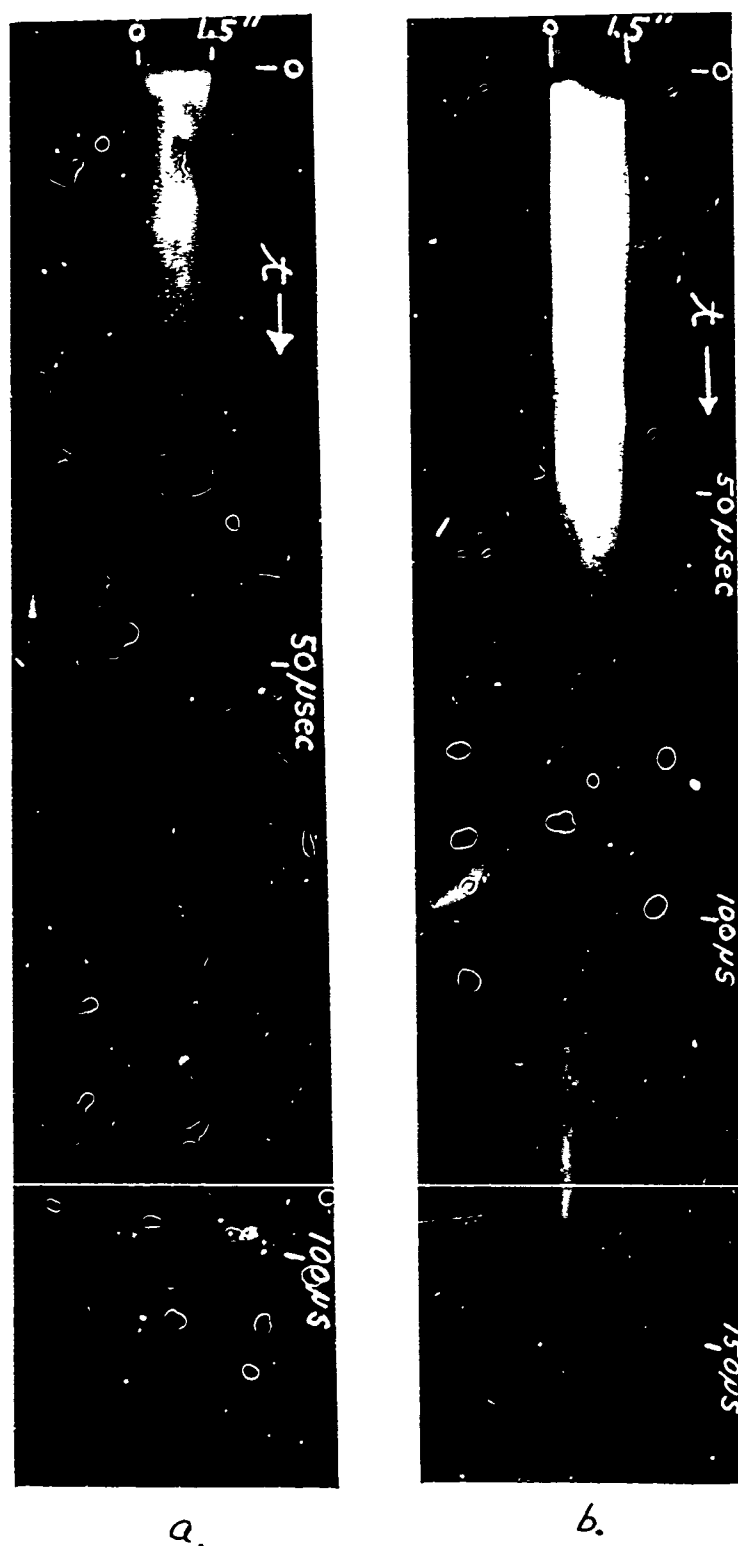
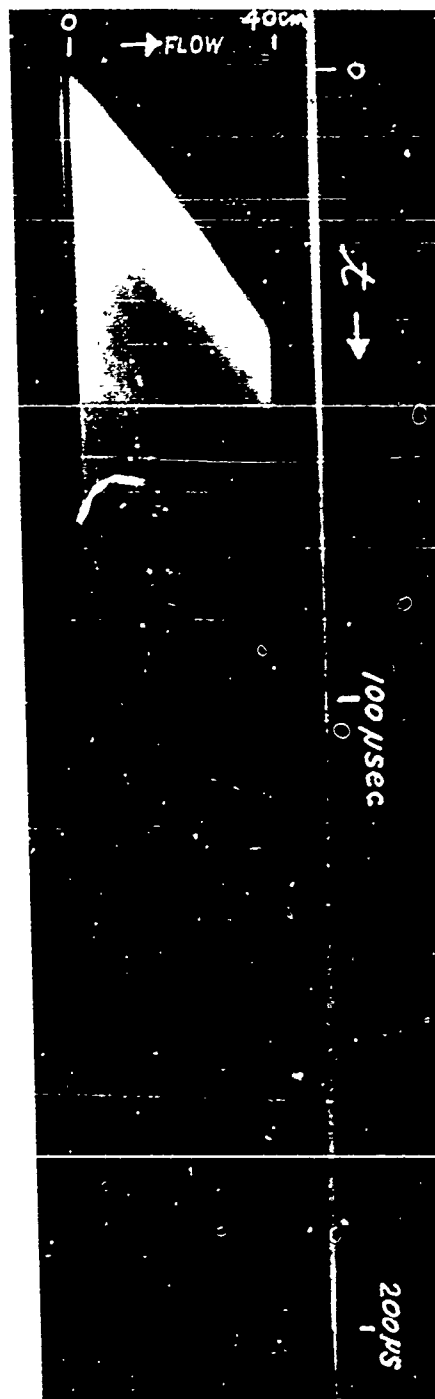


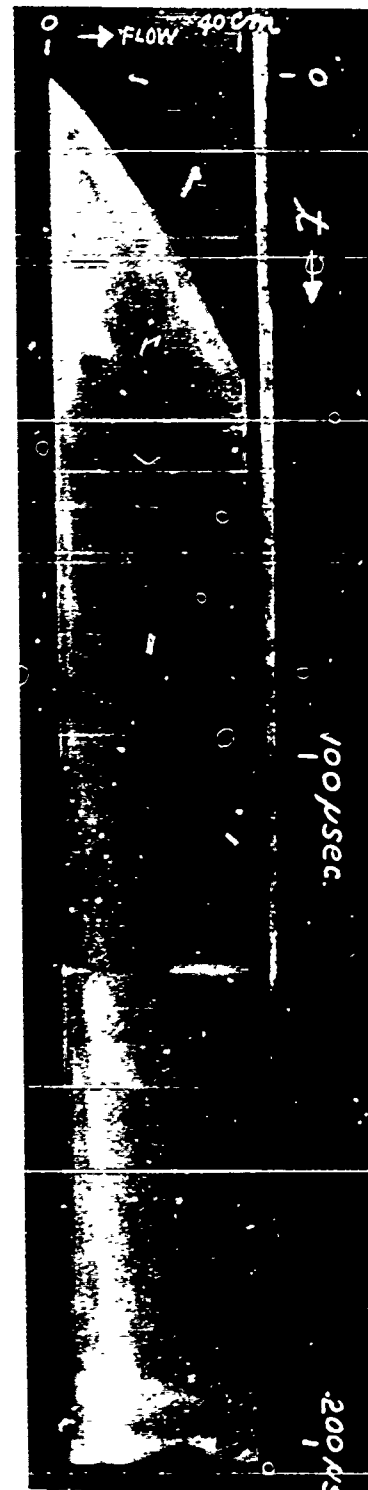
Fig. 24 Vertical smear photographs of the flow downstream of the short accelerator, about 4 diameters from station d. The working fluid was argon at  $P = 2$  mm Hg.,  $B_0 = 10$  kg. and  $J_T = 4,500$  and  $11,800$  amps for a. and b. respectively.



Fig. 25 Horizontal smear photographs of the flow downstream of the short accelerator, starting at station d, with  $B_0 = 10$  kg. and argon as the working fluid at  $p = 2$  mm Hg.  $J_T = 6,300$  and  $17,800$  amps for a. and b. respectively.



26



27

Figs. 26 and 27 Horizontal smear photographs of the flow downstream of the long accelerator starting at station d. Fig. 26 is for argon at  $p = 2$  mm Hg.,  $B_0 = 15$  kg. and  $J_T = 16,500$  amps. Fig 27 is for air at  $p = 2$  mm Hg.,  $B_0 = 10$  kg. and  $J_T = 18,000$  amps.



Fig. 28 Horizontal smear photograph of the flow downstream of the short accelerator showing a double shock in argon at  $p = 2$  mm Hg.,  $J_T = 11,400$  amps and  $B_0 = 15$  kilogauss.